JOURNAL OF PETROLOGY | VOLUME 53 | NUMBER 7 | PAGES 1505–1536 | 2012 | doi:10.1093/petrology/egs024

Elemental and Isotopic Evidence for Granitoid Genesis From Deep-Seated Sources in the Coast Mountains Batholith, British Columbia

JAMES D. GIRARDI[1], P. JONATHAN PATCHETT[1], MIHAI N. DUCEA[1]*, GEORGE E. GEHRELS[1], M. ROBINSON CECIL[1], MARGARET E. RUSMORE[2], GLENN J. WOODSWORTH[3], DAVID M. PEARSON[1], CHRISTIAN MANTHEI[1] AND PAUL WETMORE[4]

[1]DEPARTMENT OF GEOSCIENCES, UNIVERSITY OF ARIZONA, TUCSON, AZ 85721, USA

[2]DEPARTMENT OF GEOLOGY, OCCIDENTAL COLLEGE, LOS ANGELES, CA 90041, USA

[3]GEOLOGICAL SURVEY OF CANADA, VANCOUVER, BC V6B 5J3, CANADA

[4]DEPARTMENT OF GEOLOGY, UNIVERSITY OF SOUTH FLORIDA, TAMPA, FL 33620, USA

RECEIVED MAY 28, 2011; ACCEPTED FEBRUARY 28, 2012
ADVANCE ACCESS PUBLICATION APRIL 25, 2012

Major element, trace element and Nd–Sr isotopic data are presented for 82 plutonic rocks from the southern Coast Mountains Batholith (CMB) in British Columbia, Canada, ranging in emplacement age from 210 to 50 Ma. The rocks are part of a large composite magmatic arc batholith, which the major element data show to be of calc-alkaline affinity. The majority of CMB samples lack the depletion in Eu that would be consistent with equilibration of magmas and plagioclase-bearing crystalline residues or fractionates, suggesting that equilibration took place deeper than the pressure limit of plagioclase stability at 35–40 km depth. The CMB samples show a wide variation in the slope of normalized rare earth element (REE) patterns, with chondrite-normalized La/Yb ratios above 10 being mostly confined to periods of high magmatic flux in the arc at 160–140, 120–80, and 60–50 Ma. The clearest relationships between major and trace elements are negative correlations between SiO_2 and each of Sc, Y, and the heavier REE Gd to Lu. Nd and Sr isotopes mostly document juvenile origins for the granitoids, but show variations to higher $^{87}Sr/^{86}Sr$ and lower ε_{Nd} during high-flux periods. The results are interpreted to indicate a deep origin for most CMB magmas, below ~40 km where mafic to intermediate rock assemblages previously added to the arc crust by mantle melting were transformed to an (amphibole-bearing)-eclogite facies cumulate or restite, such that melting residues consisted mainly of two pyroxenes, garnet and variable proportions of amphibole. Thickened orogenic crust, for which there is clear geological evidence during the period 100–80 Ma, promoted this process. During high-flux periods, larger amounts of older rocks, mostly mafic rocks and some metasediments added to the base of the arc during orogenic shortening, became involved in magma genesis.

KEY WORDS: *British Columbia; arc magmatism; batholiths; magmatic flux; garnet; pyroxene; amphibole*

INTRODUCTION

The Coast Mountains Batholith (CMB), also referred to as the Coast Plutonic Complex, is the largest composite batholith in North America (Barker & Arth, 1984). The CMB can be traced from northern Washington for 1700 km through British Columbia, SE Alaska and into the Yukon. Owing to the nature of the accreted terranes that host the CMB, and the local deep levels of exposure in this fossil continental magmatic arc, studies of the CMB have proved invaluable to understanding Canadian Cordilleran tectonics (Armstrong, 1988; van der Heyden, 1992; Hollister & Andronicos, 2006; Gehrels *et al.*, 2009)

*Corresponding author. E-mail: ducea@email.arizona.edu

and the genesis of continental crust (Samson & Patchett, 1991; Samson *et al.*, 1991*a*; Hollister & Andronicos, 2006).

Radiogenic isotope studies, mostly Sr and Nd, have established that the accreted terranes intruded by the CMB have depleted mantle-like isotopic compositions (Samson *et al.*, 1989, 1991*b*). In Sr–Nd isotope space, predominantly mantle array-like isotope compositions (e.g. White, 1985) that range from mostly depleted mantle-like compositions, through Bulk Earth to very weakly continent-like compositions characterize the CMB, best demonstrated in southern British Columbia (Armstrong, 1988; Samson *et al.*, 1989; Cui & Russell, 1995; Friedman *et al.*, 1995). New zircon Hf isotopic data from the central–southern CMB suggest a west to east transition from slightly less depleted to more depleted Hf isotopic crustal domains that host the CMB plutons, and highly correlated Hf and Nd isotopic signatures (Cecil *et al.*, 2011).

In the northern CMB, the presence of a nearby ancient continental margin assemblage is indicated by Proterozoic detrital zircons from metamorphic rocks and similar ages of inheritance in igneous zircons from plutonic rocks (Gehrels *et al.*, 1990). Incorporation of these assemblages into the batholith may explain the more evolved Nd and Sr isotopic signatures of plutonic rocks in the northern CMB (Samson *et al.*, 1991*a*). However, the occurrence of metamorphic country rocks that in some localities have more depleted, mantle-like, isotopic compositions than the CMB intrusions themselves (Patchett *et al.*, 1998), does not support assimilation at shallow levels.

To date, magma genesis depths and sources for the CMB remain poorly constrained. Previous studies have suggested that these rocks are predominantly mantle-derived, but may contain ~10–50% recycled crustal material (Samson *et al.*, 1991*a*; Cui & Russell, 1995). The oxygen isotope data of Wetmore & Ducea (2011) appear to constrain a near-surface residence history for the recycled source materials of the CMB, especially during the initial stages of arc evolution in the Jurassic. Intracrustal assimilation and fractional crystallization (Taylor, 1980; DePaolo, 1981) and crustal anatexis (Patiño-Douce *et al.*, 1990) have been thought to provide mechanisms for generating the range of chemical and isotopic compositions seen in the CMB (Samson *et al.*, 1991*a*; Cui & Russell, 1995; Thomas & Sinha, 1999).

In this study, new Nd–Sr isotope and major and trace element data are reported for 82 plutonic rock samples from the CMB. A subset of 41 samples, 108–50 Ma in age, were studied previously by Wetmore & Ducea (2011) in an effort to characterize aspects of magmatism in the study area (Fig. 1), with a specific focus on determining the recycling of crustal components via oxygen isotopes. Another sample subset was used to characterize the Hf isotopic composition of zircons from the Gehrels *et al.* (2009) study (Cecil *et al.*, 2011). All the samples in this study have been dated using U–Pb zircon geochronology as part of prior work by Gehrels *et al.* (2009), who also characterized magmatic addition rates and the tectonic evolution of the CMB.

Samples were collected from three transects across the south–central batholith, indicated by the rectangles in Fig. 1: A, Douglas Channel in the north; B, Mathieson Channel in a central position; C, Burke–Dean Channels to the south. The rocks sampled encompass Jurassic–Eocene magmatism and span periods of terrane accretion, translation, and deformation as the western edge of NW North America was formed (Armstrong, 1988; Monger & Price, 2002).

The purpose of this study is to characterize the petrological, major and trace element and isotopic compositions of a large sample suite, 210–50 Ma in age, perpendicular to the trend of the CMB, in the general inboard (eastward) direction of arc migration. Our dataset displays relationships between major elements, rare earth elements (REE), and isotopes that have not previously been recognized in the CMB. New data presented in this study share characteristics such as a relative lack of strong Eu anomalies and wide ranges in La/Yb, Sr/Y, Nd and Sr isotopes with previous studies of large continental margin arcs (e.g. Kistler & Peterman, 1973, 1978; Gromet & Silver, 1987; Barnes *et al.*, 2006; Hildreth & Moorbath, 1988; Mamani *et al.*, 2010; Kay *et al.*, 2005). These studies, among many others, laid out the processes that may govern the production and composition of magmas in long-lived arcs. Recent models calling upon the convective rise of slab and sediment plumes into the overlying mantle wedge and their subsequent melting at subduction zones (Castro *et al.*, 2010; Hacker *et al.*, 2011) have provided new and exciting hypotheses for large-degree melting of the downgoing plate.

It will be shown that the elemental and isotopic variations provide strong constraints on the depths and sources of magmas in the CMB; such constraints are critical to understanding the evolution of magmatism in continental margin arcs.

TECTONIC SETTING

The CMB at the latitude of our study consists of three separate magmatic belts (Fig. 1) (Monger *et al.*, 1994; Gehrels *et al.*, 2009): (1) a western magmatic belt formed in the outboard Alexander and Wrangellia terranes prior to 100 Ma; (2) an eastern magmatic belt formed in the inboard Stikine and Yukon–Tanana terranes prior to 110 Ma; (3) a younger magmatic belt emplaced across much of the orogen from 100 to 50 Ma, after middle Cretaceous juxtaposition of outboard and inboard terranes (Fig. 1). The salient details of each of these three distinct arcs are presented below.

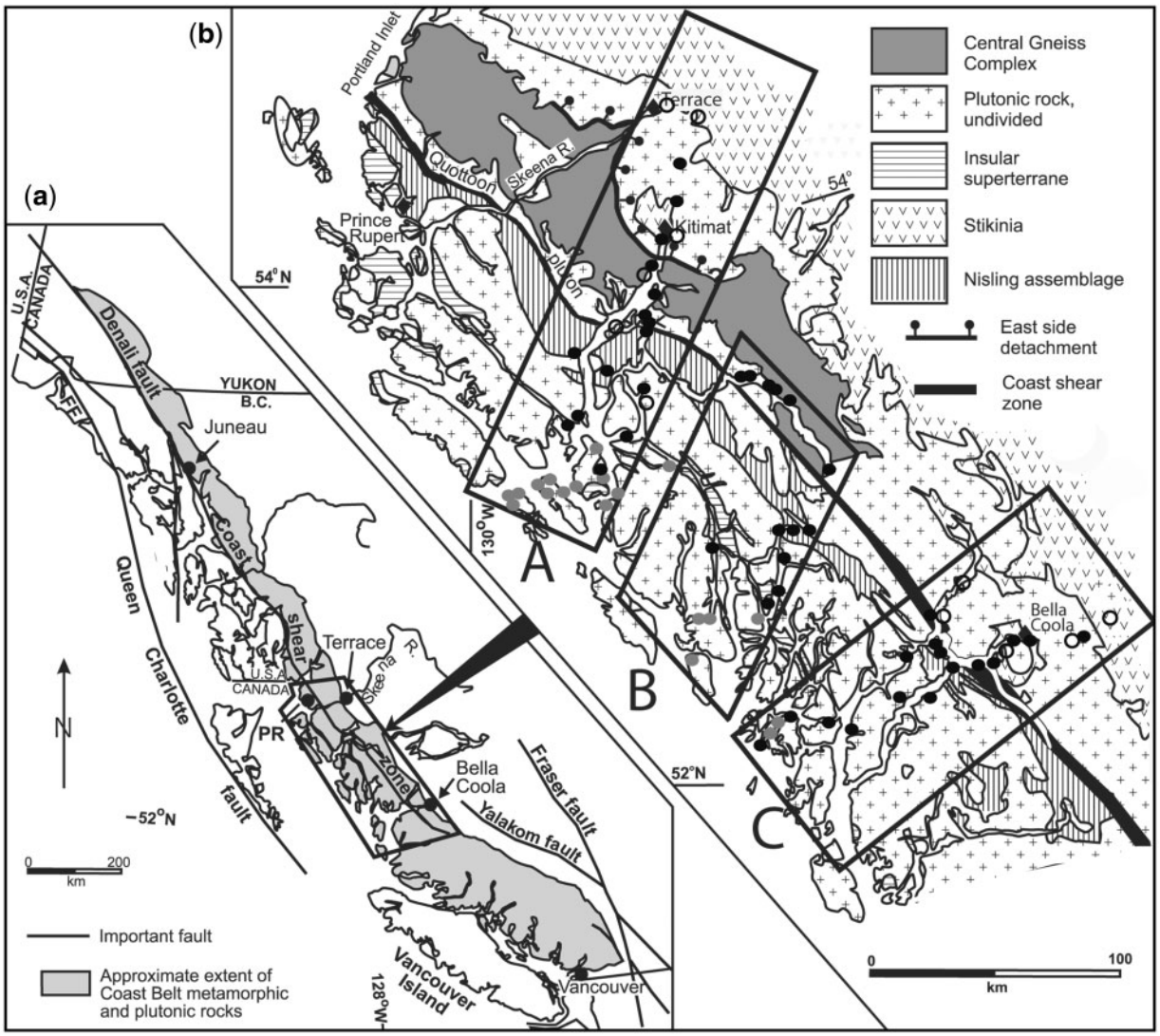

Fig. 1. Location of the study area. (a) Extent of the Coast Belt plutonic and metamorphic rocks, and major Tertiary faults. (b) Regional geological map showing sample locations (open and filled circles). Samples are located along three transects: A (northern), Douglas Channel; B (central), Mathieson Channel; C (southern), Burke–Dean Channels. Sample locations from the Outboard JK arc (gray circles), Inboard JK arc (black open circles), and post-100 Ma arc (black closed circles) are plotted along the transects. One sample, 05MT-155 (late Cretaceous in age) is from outside the transects and plots just north of the map area in Portland inlet. Geology modified from Rusmore *et al.* (2005).

Pre-100 Ma magmatic belts

Two juxtaposed Jurassic–Cretaceous arcs have been defined in the study area (Monger *et al.*, 1994; Gehrels *et al.*, 2009). One arc formed on the continental margin in the Stikine and Yukon–Tanana terranes prior to 110 Ma, and at present makes up the eastern portion of the CMB. The other arc formed outboard of the continental margin in the Alexander and Wrangellia terranes, and was juxtaposed against the Stikine and Yukon–Tanana terranes before development of the main CMB that occurred between 100 and 50 Ma (Gehrels *et al.*, 2009); this arc is now present in the western portion of the CMB. From ~100 Ma onward the CMB was part of a single contractional orogen with poorly documented transcurrent motion (Crawford *et al.*, 1987; Kapp & Gehrels, 1998; Andronicos *et al.*, 1999; Rusmore *et al.*, 2001).

To be consistent with the paleogeographical setting of each pre-100 Ma arc, our text and figures cited below will refer to these magmatic belts in the shorthand 'Outboard JK arc' for the Jurassic–Cretaceous arc located in the western portion of the CMB and 'Inboard JK arc' for the Jurassic–Cretaceous arc located in the eastern CMB.

Tectonic models for the development of the pre-100 Ma CMB vary. Monger *et al.* (1994) and Gehrels *et al.* (2009)

proposed that the Outboard JK arc was displaced from the northern CMB along sinistral faults. Alternatively, the Outboard JK arc and associated Insular superterrane (consisting of the Alexander+Wrangellia terranes) may have been accreted to the continental margin prior to mid-Jurassic times, but subsequently pulled off the margin as back-arc basins opened and then closed during mid-Cretaceous time (McClelland *et al.*, 1992; van der Heyden, 1992). Another model proposed by Monger *et al.* (1982) is that the Outboard JK arc and its Alexander–Wrangellia host-rocks were separated from the continental margin by a broad ocean basin prior to mid-Cretaceous accretion.

In all tectonic models, the Outboard JK arc formed above an eastward-dipping subduction zone between ~200 and 100 Ma (e.g. Armstrong, 1988; van der Heyden, 1992; Gehrels *et al.*, 2009). The allochthonous Outboard JK arc is exposed as plutons emplaced into metamorphic country rocks of the Alexander terrane. These include the metasedimentary Banks Island assemblage with ancient continental Nd and Proterozoic detrital zircons (Boghossian & Gehrels, 2000; Gehrels & Boghossian, 2000). Magmatism in the Outboard JK arc peaked during the period 160–140 Ma, followed by a cessation in magmatism from 140 Ma to ~120 Ma (Gehrels *et al.*, 2009). The Inboard JK arc was formed *in situ* on the margin of the Stikine terrane (Mahoney *et al.*, 2009). Plutonism in the Inboard JK (210–130 Ma) arc was persistent but with very low flux rates (Gehrels *et al.*, 2009), and the plutons are associated with and/or closely follow an intense development of Jurassic arc volcanic rocks (the Hazelton Group) (MacIntyre *et al.*, 2001).

Gehrels *et al.* (2009) noted that orthogonal convergence (Engebretson *et al.*, 1985) correlates with the high flux period in the Outboard JK arc, and that the subsequent magmatic lull correlates with a change to sinistral oblique convergence. This motion may have emplaced the Outboard JK arc against the Inboard JK arc, shutting off magmatism in the Inboard JK arc at about 110 Ma (Monger *et al.*, 1994; Gehrels *et al.*, 2009). It is not clear why magmatic production is minimal from 140 to 120 Ma, when younger periods of oblique convergence (discussed below) are synchronous with high magmatic production rates.

Eastward-younging 100–50 Ma arc

A coherent eastward-younging belt of 100–50 Ma plutons, referred to here as the 'post-100 Ma arc', was generated during and after the accretion of the Outboard JK arc (Insular superterrane) to the continental margin under dextral oblique convergence (Engebretson *et al.*, 1985; Armstrong, 1988; van der Heyden, 1992; Andronicos *et al.*, 1999; Hollister & Andronicos, 2000, 2006; Gehrels *et al.*, 2009). The post-100 Ma arc can be divided into five belts of intrusions based on geography and age (van der Heyden, 1992; Wetmore & Ducea, 2011). From west to east these belts are the western middle Cretaceous intrusions, the Ecstall-equivalent intrusions, the Coast Shear Zone intrusions, the late Paleocene to Eocene intrusions, and the eastern Late Cretaceous intrusions (Fig. 1).

Voluminous plutons were intruded across the older arcs during extensive contraction and crustal thickening in the central–southern CMB from 100 to 80 Ma (Crawford *et al.*, 1987; Rubin *et al.*, 1990; Rusmore & Woodsworth, 1991, 1994; Hollister & Andronicos, 2006; Gehrels *et al.*, 2009), producing west- and east-verging thrust belts. Hollister & Andronicos (2006) called for simultaneous translation and thickening of the crust to >55 km from 80 to 60 Ma; the beginning of this interval corresponds to the transition to low-flux magmatism that lasted until ~60 Ma, following a high-productivity period from 120 to 80 Ma (Gehrels *et al.*, 2009). The principal mechanisms responsible for crustal thickening are contraction related to the compressive regime under which the upper plate was placed during the late Cretaceous, possible tectonic accretion (underplating) from the trench side following subduction erosion, and magmatic thickening via repeated basaltic emplacement under the main arc.

The final period of increased magmatic flux, 60–50 Ma, was coincident with contraction on the Coast Shear Zone (65–55 Ma) and regional extension along the east side of the batholith (54–47 Ma). Between ~54 and 47 Ma rapid regional extension and exhumation significantly thinned the crust, and cooled and exhumed the Central Gneiss Complex (Heah, 1990, 1991; Andronicos *et al.*, 2003; Rusmore *et al.*, 2005; Hollister & Andronicos, 2006). During this period of high magmatic production (Gehrels *et al.*, 2009) the arc was transtensional owing to highly oblique convergence (Hollister & Andronicos, 2006).

In the northern and central CMB, magma emplacement was in part facilitated by extensional detachment faulting along the eastern flank of the CMB (Crawford *et al.*, 1999; Andronicos *et al.*, 2003; Rusmore *et al.*, 2005; Hollister & Andronicos, 2006). However, along the southernmost transect of this study, there is little evidence for significant crustal extension (Rusmore *et al.*, 2001, 2007). Although rapid exhumation of the CMB ended at around 48 Ma (Hollister, 1982; Rusmore *et al.*, 2005), extension and minor volcanism affected the batholith throughout the Cenozoic (Manthei *et al.*, 2010).

In addition to orthogonal convergence, there may have been major transcurrent motions along the North American margin before 100 Ma, even along the lines of the 'Baja BC hypothesis' (although with different timing), and in fact the place where the 'Outboard JK arc' formed in relation to North America is almost completely unconstrained. Nevertheless, we follow our earlier work (Gehrels *et al.*, 2009) in recognizing a coherent geological and geochemical development during the 100–50 Ma

magmatism, and we regard it as unlikely that the 100–50 Ma CMB represents segments assembled from distant parts of the continental margin, but instead that it formed more or less in place as a coherent continental arc complex.

ANALYTICAL METHODS

Major and trace elements

All rock samples were prepared at the University of Arizona using a steel jaw crusher and an Al_2O_3 mill for powdering. Splits from the same sample aliquot were used for major elements, trace elements, and radiogenic isotopes. CMB samples were analyzed for major element compositions (see Electronic Appendix 1, available for downloading at http://www.petrology.oxfordjournals.org) at Macalester College (Jeff Thole, analyst) using a Philips PW-2400 X-ray fluorescence spectrometer with Rh-anode, end-window X-ray tube, and Philips Super-Q analytical software [techniques follow Vervoort *et al.* (2007)]. Estimated 2σ uncertainty on major element oxides is ±2–4% of the values given. Trace element concentrations were analyzed at the Department of Geological Sciences, University of Saskatchewan, Canada, by inductively coupled plasma mass spectrometry (ICP-MS). The 2σ uncertainty is estimated at ±5–10% for trace elements, and ~10% on each REE. Samples were analyzed (Jianzhong Fan, analyst) by ICP-MS on a SCIEX ELAN model 250 system following the techniques of Jenner *et al.* (1990) and Longerich *et al.* (1990).

Radiogenic isotopes

Sr and Nd isotopes were measured at the University of Arizona by thermal ionization mass spectrometry methods, following Patchett & Ruiz (1987) with slight modifications explained below. Between 180 and 300 mg of sample powder were weighed and put into high-pressure Teflon vessels for dissolution in concentrated HF–HNO_3. Dissolutions were conducted at 150°C for 1 week to ensure complete digestion of refractory phases. Following dissolution, samples were dried on hot plates and re-dissolved in open Teflon vessels with 3 ml 6M HCl and 1 ml saturated H_3BO_3 in 2·5 M HCl, and then dried and re-dissolved in 6 M HCl. The 6 M HCl was evaporated off, and samples were finally dissolved in 6 M HCl, heated to 150°C overnight in closed high-pressure Teflon vessels, and then the entire solution was transferred to open beakers and spiked using ^{87}Rb–^{84}Sr and ^{149}Sm–^{150}Nd tracer solutions. After drying, the spiked samples were redissolved in 2·5 M HCl prior to loading into ion-exchange columns.

Chemical separations were performed with AG50W-X12 resin ion-exchanger in 8·9 ml quartz columns, using 2·5 M HCl as eluent for Rb and Sr, and 6·0 M HCl as eluent for bulk REE separation. Sm and Nd separations were performed using hydrogen di-2-ethylhexyl phosphate (HDEHP) adsorbed onto PTFE powder in 1·7 ml quartz columns, using 0·18 M HCl as eluent for Nd and 0·50 M HCl for Sm. Rb and Sr were loaded onto filaments as phosphate, and Sm and Nd as chloride. Sm and Nd were analyzed using a triple filament assembly with Ta sides and a Re center, and Rb on double Ta filaments, using a VG-354 mass spectrometer. Sr was analyzed using single Ta filaments and a Micromass SECTOR 54 mass spectrometer. During the measurement period, repeated measurements of the NBS-987 Sr standard yielded $^{87}Sr/^{86}Sr$ of $0{\cdot}710229 \pm 11$ ($n = 11$) for ratios normalized to $^{86}Sr/^{88}Sr = 0{\cdot}1194$. Repeated measurements of the La Jolla Nd standard yielded $^{143}Nd/^{144}Nd$ of $0{\cdot}511869 \pm 9$ ($n = 18$) for ratios normalized to $^{146}Nd/^{144}Nd = 0{\cdot}7219$. Total procedural blanks during the measurement period were <100 pg for Sr and < 50 pg for Nd and Sm. Uncertainties of $^{87}Sr/^{86}Sr$ and $^{143}Nd/^{144}Nd$ are reported as $2\sigma_m$; all data are given in Electronic Appendix 1.

RESULTS

Petrography

The rocks investigated in this study range from gabbro to granodiorite, with diorite to tonalite compositions being the most common. Wetmore & Ducea (2011) described a subset of the samples from those described here. The samples are granular, medium to coarse grained, and consist primarily of quartz, plagioclase feldspar, alkali feldspar and the mafic minerals amphibole, biotite, and sparse pyroxene in diorite–gabbros. Accessory minerals apatite, titanite, and zircon are common. One group of samples, equivalent to the Ecstall intrusions (Hutchison, 1983; Zen & Hammarstrom, 1984; Butler *et al.*, 2002) are characterized by 2% or less of primary magmatic epidote. Fe–Ti oxides are common in many of the samples in this study, with the exception that they are sparse in most granodiorites, and especially in the granites that were produced only during Paleocene–Eocene times. Trace amounts of garnet were observed in one of the eastern late Cretaceous intrusions and also in one of the Paleocene intrusions.

Granitoids rich in both modal quartz (>20%) and alkali feldspar (>10%), of tonalitic to granodioritic composition, were generated in the Outboard JK arc, Inboard JK arc, and in the post-100 Ma arc. However, prior to the post-100 Ma arc, such compositions are not well correlated with age or location. One pluton within the eastern late Cretaceous intrusions and several plutons of the Paleocene–Eocene intrusions contain muscovite.

The elemental and isotopic data discussed below are presumed to closely approximate initial magmatic compositions. Pluton sample locations were chosen because they exhibited limited internal differentiation or accumulation of fractionates, and mafic enclaves were sparse or absent. In addition, petrographic observations indicate

Table 1: Major element (wt %) compositions of representative samples from this study

Sample	Group	Rock type	Age (Ma)	SiO_2	TiO_2	Al_2O_3	Fe_2O_3*	MnO	MgO	CaO	Na_2O	K_2O	P_2O_5	LOI	Total	A/CNK	Mg#
04GJP-16	Ei	Granite	52·6 ± 1·5	72·71	0·13	15·45	1·14	0·03	0·30	1·84	4·86	2·91	0·04	0·34	99·74	1·05	34
04GJP-14	CSZi	Tonalite	58·4 ± 1·9	61·26	0·99	16·35	6·17	0·09	2·57	4·98	4·28	1·95	0·35	0·50	99·47	0·89	45
04GJP-22	ELK	Qtz. diorite	61·5 ± 1·6	63·10	0·64	17·27	4·77	0·09	2·20	4·90	4·45	1·94	0·19	0·48	100·04	0·92	48
04GJP-8	ELK	Qtz. diorite	68	60·72	0·85	16·53	6·59	0·10	2·97	5·90	4·15	2·01	0·29	0·22	100·32	0·82	47
04GJP-83	EI	Tonalite	80·7 ± 1·6	65·77	0·49	16·69	4·11	0·07	1·75	4·70	4·01	1·50	0·17	0·40	99·66	0·97	46
04GJP-71	EI	Tonalite	82·6 ± 1·1	64·08	0·67	16·79	4·65	0·07	2·13	4·83	4·15	2·03	0·18	0·40	99·98	0·92	48
04GJP-36	EI	Tonalite	92·2 ± 2·5	64·03	0·62	17·93	3·79	0·07	1·36	4·68	5·31	1·95	0·19	0·35	100·27	0·91	42
04GJP-78	ELK	Granodiorite	96·8 ± 2·1	63·34	0·50	17·71	4·83	0·11	1·93	5·19	4·34	1·50	0·25	0·34	100·05	0·95	44
04GJP-68	WMK	Tonalite	97·1 ± 1·2	59·33	0·92	16·58	6·71	0·12	3·62	5·99	3·90	2·32	0·30	0·58	100·38	0·82	52
05MT-112	OJK-WMK	Qtz. diorite	103·4 ± 1·5	59·93	0·56	17·42	7·30	0·17	2·89	7·08	3·37	1·64	0·18	0·59	100·52	0·83	44
04GJP-39	OJK-eK	Qtz. diorite	116·4 ± 3	70·89	0·46	14·47	3·22	0·07	1·20	3·27	3·88	2·63	0·12	0·61	100·81	0·93	42
04GJP-89	IJK-eK	Tonalite	130·2 ± 1·9	66·60	0·35	17·30	3·20	0·08	1·63	4·64	4·66	1·25	0·15	0·36	100·22	0·97	50
04GJP-56	OJK-eK	Granodiorite	142·5 ± 2	69·16	0·29	16·65	2·55	0·07	0·82	3·82	4·55	1·71	0·11	0·26	99·99	1·00	39
04GJP-57	OJK-lJ	Tonalite	146·7 ± 2·1	66·99	0·37	17·02	3·24	0·07	1·27	4·23	4·51	1·49	0·14	0·63	99·95	0·99	44
04GJP-52	OJK-lJ	Qtz. diorite	149	59·32	0·78	17·01	6·17	0·12	3·73	5·19	3·63	1·71	0·22	2·32	100·22	0·96	55
04GJP-24	IJK-mJ	Qtz. diorite	157·2 ± 2·9	63·54	0·66	15·45	5·48	0·10	2·34	4·85	3·36	2·97	0·18	0·41	99·35	0·86	46
04GJP-27	IJK-mJ	Qtz. diorite	182·3 ± 4·7	60·71	0·74	16·21	6·96	0·17	2·65	6·12	3·36	1·75	0·17	1·77	100·61	0·84	43

Ei, Eocene intrusions; CSZi, Coast Shear Zone intrusions; ELK, Eastern late Cretaceous intrusions; EI, Ecstall intrusions; WMK, Western middle Cretaceous intrusions; OJK, Outboard Jurassic–Cretaceous; IJK, Inboard Jurassic–Cretaceous; eK, early Cretaceous; mJ, middle Jurassic; lJ, late Jurassic. Ages are U–Pb zircon ages as reported by Gehrels *et al.* (2009). Alumina Saturation Index, A/CNK, is the molar ratio of $Al_2O_3/(CaO + Na_2O + K_2O)$. Mg# = molecular MgO/(MgO + FeO); FeO calculated as $0·899 \times Fe_2O_3$*.

that the primary igneous minerals are largely unaffected by hydrothermal or metamorphic processes that would modify rock compositions.

Major and trace elements

Major and trace elemental data are available for all but three samples, and are reported in Supplementary Data Electronic Appendix 1. Representative analyses are reported in Table 1, and for geochemically anomalous samples in Table 2. Representative rare earth elemental analyses are given in Table 3, and their corresponding Sr and Nd isotopic ratios are given in Tables 4 and 5 (see analytical details below). We also report major, trace, and REE chemistry set of anomalous samples (described below) in Tables 6, 7, and 8, respectively. Their corresponding Sr and Nd isotopic ratios are given in Table 9 and 10. As part of this study, 82 samples were analyzed, with 20 belonging to the Outboard JK arc, 10 from the Inboard JK arc, and 52 from the post-100 Ma arc.

The rocks of each arc are calc-alkalic, with some exceptions, based on the modified alkali–lime index defined by Frost *et al.* (2001) (Fig. 2a). Two ~86 Ma granodiorite samples, each with SiO_2 of around 75 wt % are alkali–calcic. Three other samples, a 100 Ma granodiorite, a 53 Ma tonalite, and a 153 Ma gabbro from the outboard arc, are calcic. The rock compositions form a smooth trend in alumina saturation index from 0·7 to 1·1, with the majority of rocks being metaluminous (Fig. 2b). Some samples with SiO_2 >68% are mildly peraluminous; these are mostly from the post-100 Ma Cretaceous to Eocene CMB (16 samples), but also from the Outboard JK arc (five samples), and Inboard JK arc (one sample). The average SiO_2 content in the Cretaceous to Eocene arc is 65·6 wt %, with a total alkali content ($Na_2O + K_2O$) of 6·1 wt %. This is more silicic and more alkaline than either the Inboard JK arc (SiO_2 = 64 wt %, $Na_2O + K_2O$ = 6·1 wt %) or Outboard JK arc (SiO_2 = 61·7 wt %, $Na_2O + K_2O$ = 5·6 wt %).

Mid-ocean ridge basalt (MORB)-normalized (Pearce, 1983) trace element patterns (Fig. 3) show very similar behavior for all three granitoid groups, shown in gray, and representative samples (Table 2), shown in black. As in the more limited dataset of Wetmore & Ducea (2011), all the CMB samples from this study show negative anomalies for Nb and Ta. The elements Th, P, Ti, Y, and Yb are variable within each of the Outboard JK arc, Inboard JK arc, and post-100 Ma arc sample groups (Fig. 3). The post-100 Ma arc is overall more depleted in Y and Yb compared with the Outboard JK and Inboard JK arcs (Fig. 3). A notable distinction in the post-100 Ma arc is a

Table 2: Trace element (ppm) compositions of representative samples from this study

Sample	Group	Sr	Rb	Ba	Th	U	Ta	Nb	Zr	Hf	Y	Co	Cr	Sc	Sr/Y
04GJP-16	Ei	674	71	1345	1·6	0·3	0·2	2·1	65	2·3	4	1	10	13	157
04GJP-14	CSZi	883	37	882	1·7	0·8	0·5	7·0	103	3·1	13	15	24	16	67
04GJP-22	ELK	855	39	935	4·4	1·3	0·5	4·5	61	1·8	9	12	16	19	91
04GJP-8	ELK	621	55	682	5·8	1·6	0·3	5·9	178	5·1	18	21	31	24	34
04GJP-83	EI	587	39	672	3·8	0·4	0·2	4·3	62	1·8	7	11	27	22	78
04GJP-71	EI	651	50	1000	4·1	1·8	0·3	5·8	112	3·2	13	14	30	23	51
04GJP-36	EI	827	37	986	3·5	1·4	0·5	6·8	91	2·8	7	10	18	18	110
04GJP-78	ELK	773	39	998	8·2	0·5	0·2	6·7	157	3·9	15	10	19	27	51
04GJP-68	WMK	800	55	1240	5·2	2·1	0·8	12·7	170	4·6	22	18	61	23	36
05MT-112	OJK-WMK	534	38	647	4·0	2·0	0·5	7·4	129	3·2	18	18	9	26	30
04GJP-39	OJK-eK	416	43	906	7·9	2·2	1·1	11·7	106	3·3	12	7	18	18	34
04GJP-89	IJK-eK	884	43	592	2·9	1·5	0·4	4·9	74	2·1	11	8	34	28	80
04GJP-56	OJK-eK	754	46	649	2·1	0·4	0·9	12·6	122	3·1	12	5	11	15	65
04GJP-57	OJK-lJ	765	42	571	4·7	0·6	0·2	7·6	154	3·9	7	8	23	17	111
04GJP-52	OJK-lJ	621	52	837	8·0	1·9	0·8	12·5	160	4·0	19	22	38	28	34
04GJP-24	IJK-mJ	505	67	1080	8·3	3·4	0·5	5·3	140	4·2	15	17	57	19	33
04GJP-27	IJK-mJ	408	37	760	2·4	1·1	0·3	3·8	112	3·3	26	18	16	27	16

wider range of negative Ti anomalies; the samples with low Ti typically contain >72% SiO_2 (Fig. 4).

Correlations with silica

Harker diagrams show very similar variations for the Outboard JK arc, the Inboard JK arc, and the post-100 Ma arc, for all major oxides with silica (Fig. 4). The Outboard JK arc, Inboard JK arc, and post-100 Ma arc each display the same trends of near linear negative correlations with SiO_2 for all major element oxides except K_2O, which is positively correlated, and Na_2O, which has no clear correlation (Fig. 4). Mg-numbers [100 times molecular MgO/(MgO + FeO)] are 58 to 40 for rocks with SiO_2 up to 65%, and then decrease to 30 and lower, especially for rocks with ~75% SiO_2 (Fig. 5). The Mg-number data shown in Fig. 5 overlap for all three arcs, except for two outliers: a 83 Ma granodiorite, and a 145 Ma granodiorite from the Outboard JK arc.

Correlations between SiO_2 and Ba, Nb, Co, Sc, and Y are shown in Fig. 5 to illustrate the behavior of certain groups of trace elements in CMB magmas. Several incompatible trace elements show reasonably strong positive correlations with SiO_2, including the large ion lithophile elements (LILE) Rb, Ba, Th, and Pb. A group of trace elements is essentially uncorrelated with SiO_2, namely the high field strength elements (HFSE) Zr, Hf, Nb, Ta, and U. Elements that show negative correlations with increasing SiO_2 include the transition metals Sc, Ti, V, Cr, Co, Ni, Cu, Zn, and Y, as well as P.

Rare earth elements

Correlations with silica

The light REE (LREE) La to Pr, illustrated by La in Fig. 5, are uncorrelated with SiO_2. The heavier REE, Gd to Lu, show consistent negative correlations with SiO_2, as demonstrated by Gd and Yb (Fig. 5). The relations of SiO_2 with Eu anomaly (Eu/Eu*) as well as with $(La/Yb)_N$ are shown in Fig. 6. We estimate the 2σ uncertainty on each REE to be <10%, and about 3% uncertainty on Eu/Eu*. Average Eu/Eu* for the Outboard JK arc, Inboard JK arc, and post-100 Ma arc, are 1·00, 0·84, and 0·95, respectively. Most samples have Eu/Eu* values between 0·8 and 1·2, regardless of SiO_2 content (Fig. 6a).

Conspicuous outliers with low Eu/Eu* in Fig. 6a include a mafic enclave and seven granite samples with Eu/Eu* < 0·65 and SiO_2 > 70 wt %. The latter group includes Jurassic, middle Cretaceous and late Cretaceous or Tertiary samples, having in common that they are all among the highest-SiO_2 rocks in their age group and region. Included among these are an early middle Cretaceous granodiorite from the Outboard JK arc, two samples of the Inboard JK arc early Jurassic intrusions near Kleanza Creek (Douglas transect, Fig. 1), and four muscovite-bearing plutons.

Outliers in Fig. 6a with Eu/Eu* > 1·2 include four high-silica (>67%) intrusions from the post-100 Ma arc, which are tonalites–granodiorites from the Paleocene–Eocene intrusion suite, and a 94 Ma quartz diorite. For the samples of this study there is considerable overlap

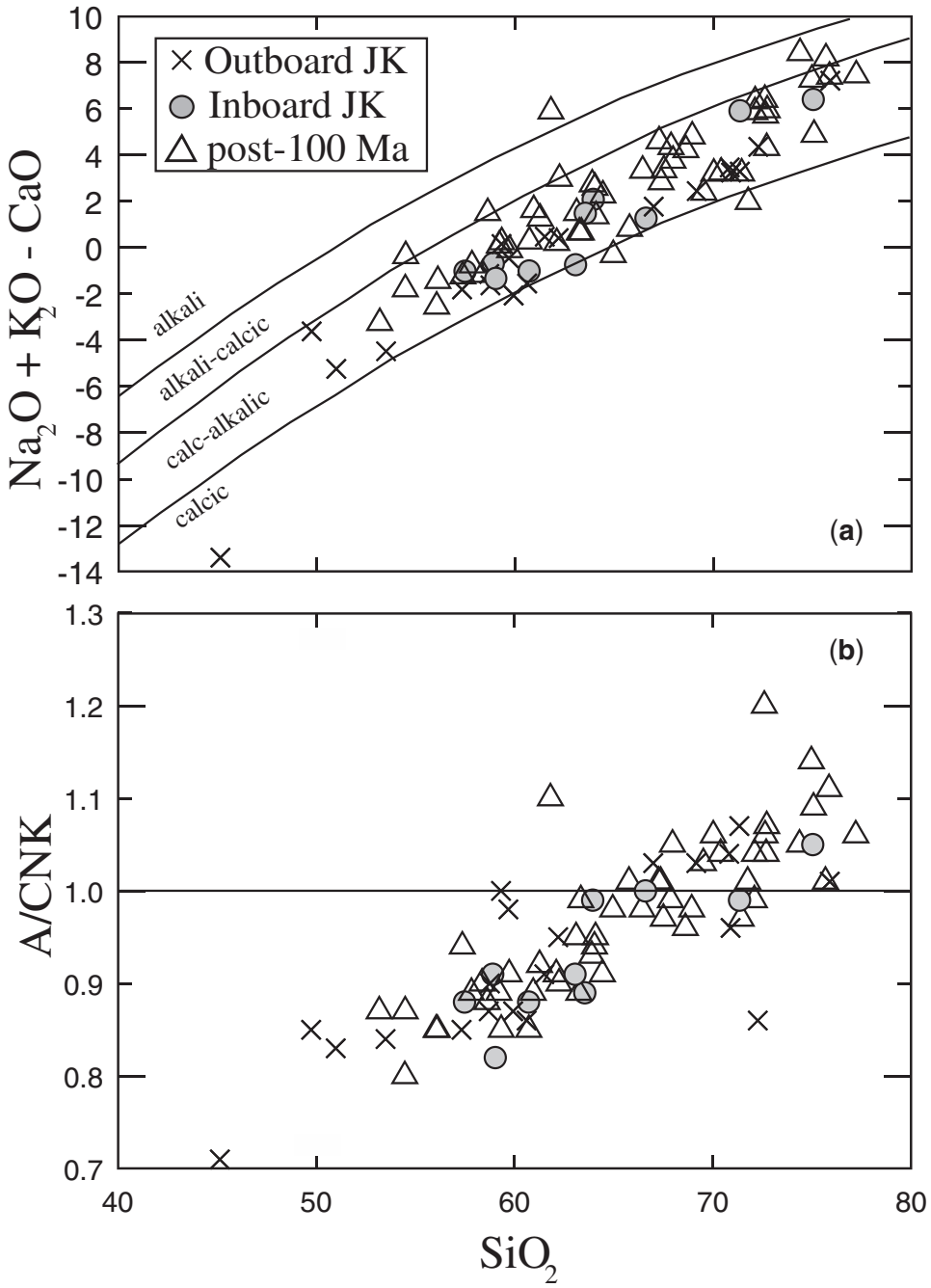

Fig. 2. The alkali–lime index (Frost *et al.*, 2001) (a), and the alumina saturation index [molar $Al_2O_3/(CaO + Na_2O + K_2O)$, A/CNK] (b) plotted against wt % SiO_2.

between the three distinct arcs, with many of the outliers of anomalously high or low Eu/Eu* associated with high-silica intrusions (Fig. 6a).

Average $(La/Yb)_N$ is 11·9, 6·3, and 15·2, respectively, for the Outboard JK arc, Inboard JK arc, and post-100 Ma arc. The relationship between $(La/Yb)_N$ and SiO_2 is shown in Fig. 6b. In the Outboard JK arc $(La/Yb)_N$ is typically <10, for SiO_2 below 60 wt %, and commonly > ~15 for $SiO_2 > 60$ wt %. There is an overall positive correlation between silica and La/Yb for each group of samples in the range of 60–70% SiO_2, the range of silica that characterizes most of our samples. Higher silica rocks are typically small-volume fractionates or late partial melts that do not exhibit the enrichment in LREE. The Inboard JK arc consistently has the lowest overall $(La/Yb)_N$, with only one sample with $(La/Yb)_N > 10$, and no correlation with

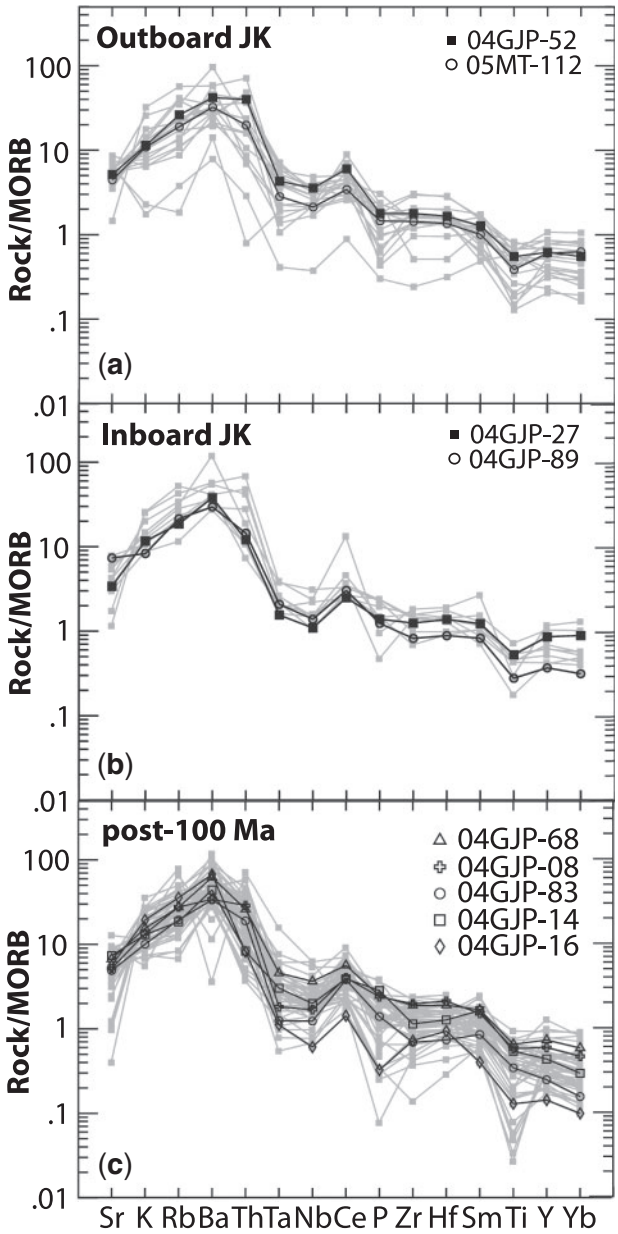

Fig. 3. MORB-normalized trace element variation diagrams for (a) the Outboard JK arc, (b) the Inboard JK arc, and (c) the post-100 Ma arc. MORB normalizing values are from Pearce (1983). All samples for each group are shown in gray; representative samples are shown in black. For the post-100 Ma arc, representative samples are from the Western middle Cretaceous intrusions (04GJP-68), Eastern late Cretaceous intrusions (04GJP-08), Ecstall-equivalent intrusions (04GJP-83), Coast Shear Zone intrusions (04GJP-14), and late Paleocene–Eocene intrusions (04GJP-16).

SiO_2 wt %. Despite having the highest average $(La/Yb)_N$, the post-100 Ma arc has $(La/Yb)_N$ that spans a wide semi-continuous range of ~5 to ~20 for all SiO_2 wt %. A small group of samples have $(La/Yb)_N > 30$. By plotting La_N and $(La/Sm)_N$ against $(Sm/Yb)_N$, as in Fig. 6c and d, additional aspects of the REE patterns can quantified. Figure 6d, which is contoured for the limits of samples with $(La/Yb)_N$ of 10, 20, and 30, shows that the slope of the REE patterns, expressed as $(La/Yb)_N$, appears to be affected by both LREE enrichment $[(La/Sm)_N]$, and heavy REE (HREE) depletion $[(Sm/Yb)_N]$. The Inboard JK arc has the most restricted range of $(Sm/Yb)_N$, and overall the lowest La_N (Fig. 6c) and $(Sm/Yb)_N$ (Fig. 6d). Samples from the Outboard JK arc fall into two groups: one group with a wide range in $(Sm/Yb)_N$, $La_N > 100$ and $(La/Sm)_N > 5$; the other group has restricted $(Sm/Yb)_N$ clustering at ~2, $La_N < 100$, and $(La/Sm)_N < 5$ (Fig. 6d). For $(La/Sm)_N < 6$ the post-100 Ma CMB consistently has the greatest $(Sm/Yb)_N$ compared with data from the Inboard JK arc and Outboard JK arc (Fig. 6d).

Chondrite-normalized REE patterns

Chondrite-normalized (McDonough & Sun, 1995) REE patterns for the Outboard JK arc, Inboard JK arc, and post-100 Ma arc are shown in Fig. 7. All data from each arc are shown in gray; representative samples are shown in black (Fig. 7). The patterns display the lack of significant Eu anomalies discussed above, and a variation in steepness of normalized abundance from La to Lu. For each arc it is clear that there exist distinct sub-sets of samples that have $(La/Yb)_N$ either greater or less than 10 (Fig. 7). Within the sub-groups, REE patterns are overall similar for all samples of this study. Several samples show an additional distinctive characteristic of their REE patterns consistent with magmas that have undergone hornblende fractionation: a concave-upward pattern from the middle REE (MREE) to HREE (Romick *et al.*, 1992).

Sr/Y ratios

Samples from this study have Sr/Y mostly in the range of 10–100, and average Sr/Y for the Outboard JK, Inboard JK, and post-100 Ma CMB are 49·7, 32·2, and 63·8, respectively. Figure 8a, a plot of Sr/Y vs Y concentration, shows that most of the analyzed samples fall in the field of loosely defined adakites (Drummond & Defant, 1990), which are thought to be melts in equilibrium with a garnet-rich or eclogite phase mineralogy (Tulloch & Kimbrough, 2003; Gao *et al.*, 2007; Richards & Kerrich, 2007). Although Sr/Y increases overall with increasing silica, it spans a wide range for intermediate to silicic samples (Fig. 8b). Samples that lie off the general trend of increasing Sr/Y with SiO_2 are characterized by $Sr/Y < \sim 20$ and $SiO_2 > 70\%$; this group consists mostly of the anomalous samples, identified earlier, that have $Eu/Eu^* < 0{\cdot}65$. Also included are 05MT-105, an 83 Ma granodiorite that is anomalous among the CMB samples in containing a large population of older (~400 Ma) inherited zircons (Gehrels *et al.*, 2009), and 05MT-101, an 85 Ma granodiorite with an anomalous alkali–calcic composition.

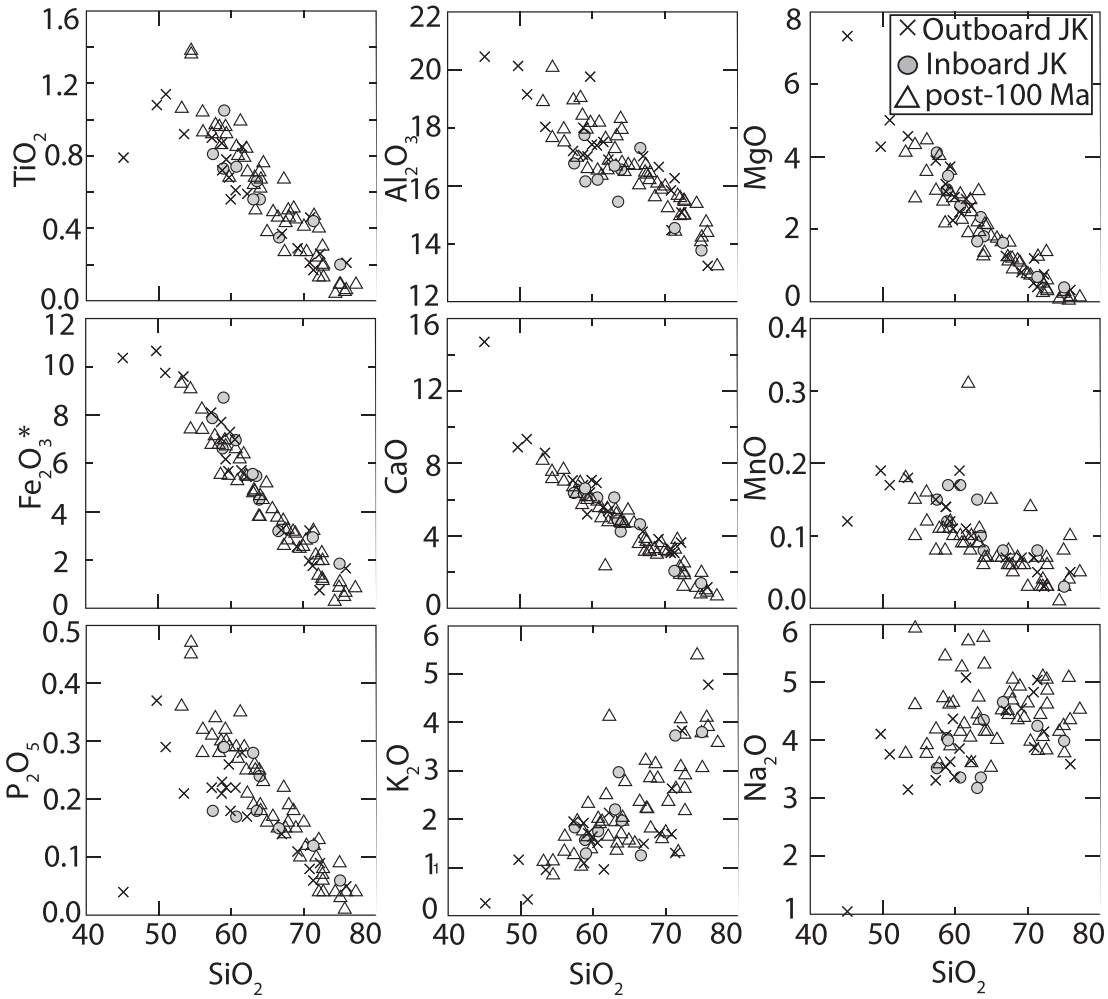

Fig. 4. Major element Harker diagrams of wt % TiO_2, Al_2O_3, MgO, Fe_2O_3*, CaO, MnO, P_2O_5, K_2O, and Na_2O vs wt % SiO_2. Fe_2O_3* is total Fe as Fe_2O_3.

Sr and Nd isotope geochemistry

Sr and Nd isotopic data are given in Supplementary Data Electronic Appendix 1. Representative compositions are reported in Tables 4 and 5, and geochemically anomalous samples in Tables 9 and 10. The Outboard JK arc, Inboard JK arc, and post-100 Ma arc show similar ranges of isotopic values for the bulk of the samples (Fig. 9). The majority of our samples are isotopically primitive, as has been documented elsewhere in the CMB (e.g. Samson *et al.*, 1989, 1991*a*, 1991*b*; Cui & Russell, 1995). We refer to 'primitive' isotopic signatures as those reflecting a reservoir that has been isolated relatively recently (<500 Ma) from the convective mantle; a source reservoir like this can be either the mantle lithosphere or could have had a near-surface crustal evolution as clearly documented for at least some of our samples (Wetmore & Ducea, 2011).

The Outboard JK and Inboard JK arc segments, located within the Insular superterrane and the Stikine terrane respectively, are shown in Fig. 9a. Although the Inboard JK arc at present lies closer to the North American continent, it is more primitive isotopically, with an initial ε_{Nd} of +3 to +8 and $^{87}Sr/^{86}Sr$ down to 0·7031. In the Inboard JK arc, initial $^{87}Sr/^{86}Sr$ is most variable and elevated in the early Jurassic, but in all cases is <0·7041, except for one sample, a 210 Ma granodiorite with $^{87}Sr/^{86}Sr$ ~0·7044. The Outboard JK arc has initial ε_{Nd} between −2 and +4 and $^{87}Sr/^{86}Sr$ between 0·7035 and 0·7062. Nd and Sr isotopes for the post-100 Ma arc span a broadly similar range compared with the pre-100 Ma arcs, and have initial ε_{Nd} ranging from −2 to +7 and $^{87}Sr/^{86}Sr$ mostly between 0·7033 and 0·7060 (Fig. 9b).

Six samples have initial ε_{Nd} below +1 and/or $^{87}Sr/^{86}Sr$ above 0·7052. The most extreme sample, a 83 Ma granodiorite with 75% SiO_2, has initial ε_{Nd} and $^{87}Sr/^{86}Sr$ of −3·5 and 0·70915, respectively. This sample is anomalous in Fig. 9b and stands out among all the CMB samples in containing a large population of older (~400 Ma)

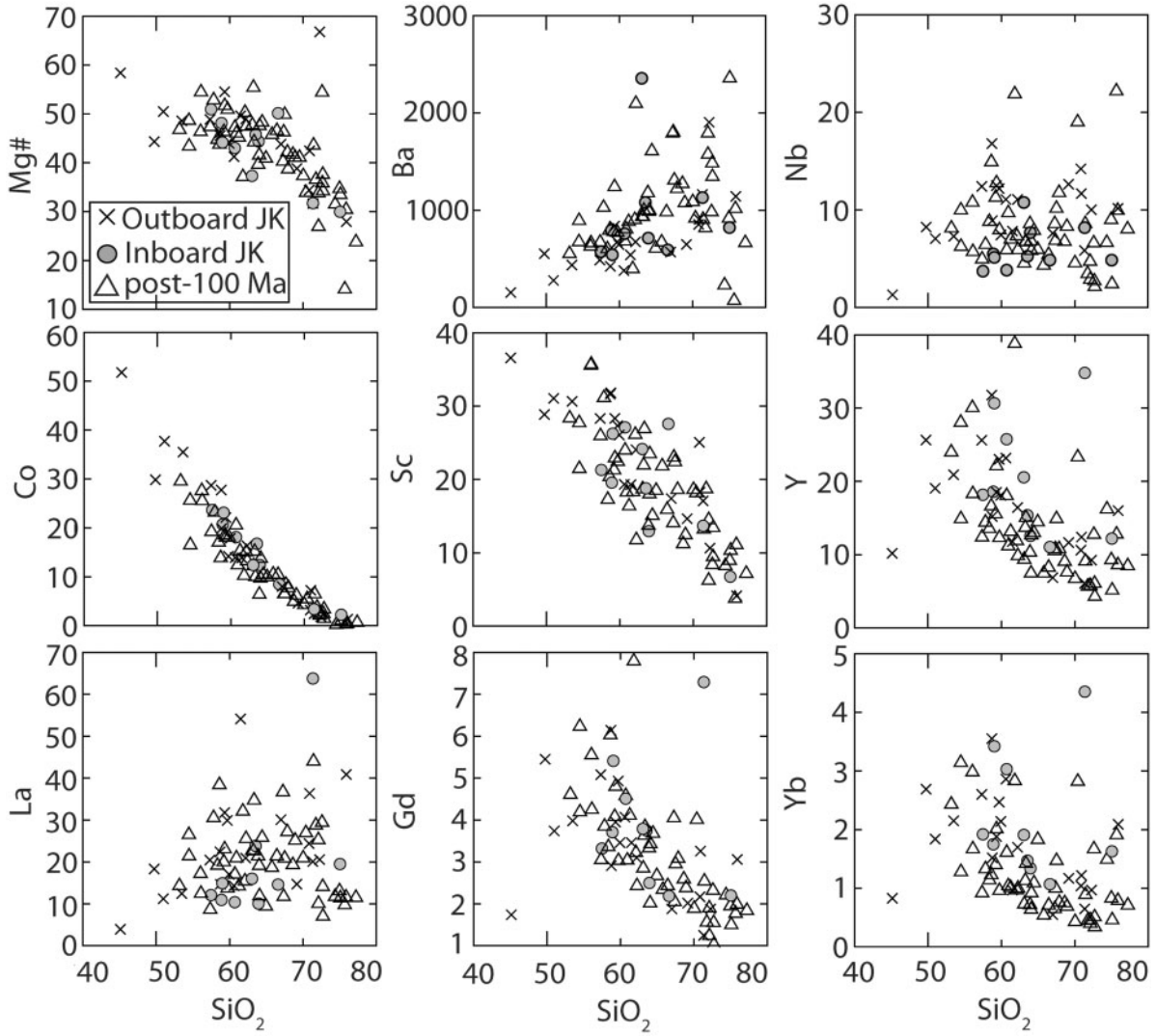

Fig. 5. Harker variation diagrams of Mg# [molecular MgO/(MgO + FeO); FeO calculated as 0·899 × Fe_2O_3*] and the trace elements Ba, Nb, Co, Sc, Y, La, Gd, and Yb (ppm concentrations) vs wt % SiO_2.

inherited zircons (Gehrels *et al.*, 2009). Other samples with anomalous ε_{Nd} or $^{87}Sr/^{86}Sr$ are a 153 Ma gabbro from the Outboard JK arc with 45% SiO_2 (04GJP-50), which is anomalous on many geochemical plots, and three Paleocene to Eocene tonalite–granodiorites with $SiO_2 > 67\%$.

Figures 10–12 show $(La/Yb)_N$, $^{87}Sr/^{86}Sr$ and ε_{Nd} plotted against age and the magmatic flux data of Gehrels *et al.* (2009); these relations will be discussed below.

INTERPRETATION OF GEOCHEMICAL DATA

Major and trace elements

To make broad observations across the composite CMB, our study has have been limited to one representative sample per pluton, and as such we are not able to evaluate magmatic processes, such as assimilation or fractional crystallization, that are specific to single magma bodies. However, what is possible, if there are substantial common elements between the parental magmas, is to address magmatic processes on the much larger scale of the arc as a whole. We feel justified in assuming a commonality between the parental magmas of the majority of the samples in this study; our rationale is explained below.

Well-defined linear trends between major element oxides and silica exhibit substantial overlap for samples of the Outboard JK arc, Inboard JK arc, and post-100 Ma arc (Fig. 4). In addition, linear and near-linear correlations between silica and Mg#, Co, Sc, Y, Gd, and Yb (Fig. 5), as well as similar MORB-normalized trace element patterns (Fig. 3), are observed for the Outboard JK arc,

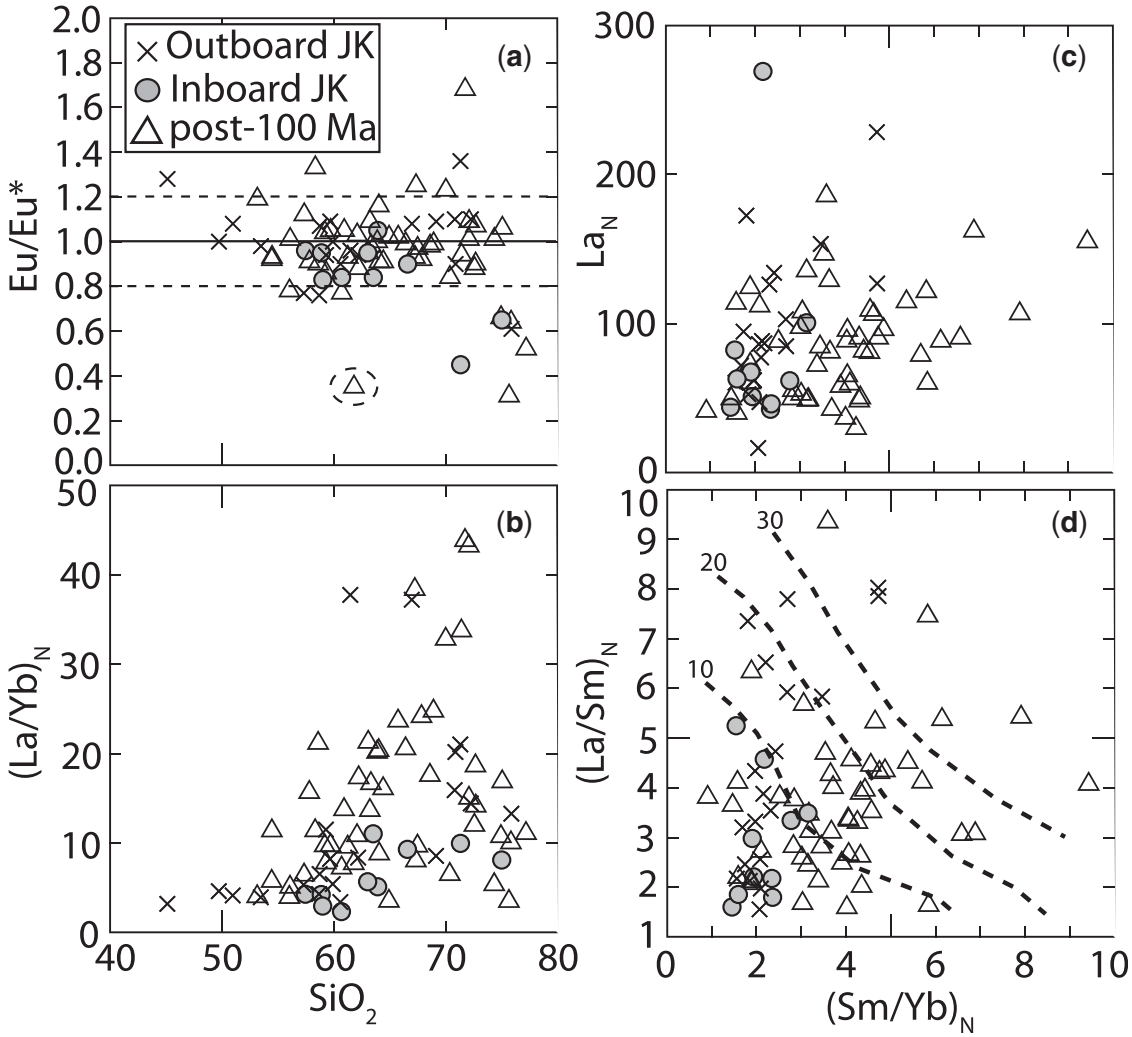

Fig. 6. The variation of Eu divided by Eu expected from interpolation of chondrite-normalized (McDonough & Sun, 1995) Sm and Gd (Eu/Eu*) (a), and La/Yb [$(La/Yb)_N$] (b), with wt % SiO_2. (c) and (d) respectively show the relation of chondrite-normalized La (La_N) and La/Sm [$(La/Sm)_N$], to chondrite-normalized Sm/Yb [$(Sm/Yb)_N$]. Horizontal dashed lines in (a) show probable ~20% uncertainty on a Eu/Eu* value of 1·0; the circled sample is 04GJP-06, a mafic enclave. Dashed lines in (d) represent contours for $(La/Yb)_N$ of 10, 20, and 30, for samples of this study.

Inboard JK arc, and post-100 Ma arc. These data broadly support the interpretation that the magmas experienced comparable histories following extraction from their sources; the coherent correlations also limit large amounts of crystal fractionation in most cases, or the involvement of assimilants with contrasting characteristics. We explore these processes in more detail below.

Clearly, there may be some exceptions that experienced magmatic processing that was different from the majority of the sampled plutons. The samples with high SiO_2 wt % and low Eu/Eu* shown in Fig. 6d are exceptional because they show the expected Eu anomaly from plagioclase fractionation, or melt extraction from a source region where plagioclase was stable. Despite similar trends among major and trace elements there are several variable geochemical characteristics of the Outboard JK arc, Inboard JK arc, and post-100 Ma arc magmas, namely Eu/Eu* and REE patterns (Figs 6 and 7), $(La/Yb)_N$ (Figs 6 and 10), Sr/Y (Fig. 8), and Sr and Nd isotopes (Figs 9, 11, and 12). These geochemical variations do not preclude a relatively uniform parental magma with regard to its major element composition, and are interpreted to reflect minor temporal and along-strike heterogeneities in magma sources, depth of magma genesis, and magmatic reworking of the lower crust over ~150 Myr.

Eu/Eu* behavior—a constraint on the depth of melting

Excluding 12 granitoid samples with Eu anomalies, most of which have $SiO_2 > 70\%$, and a mafic enclave, all

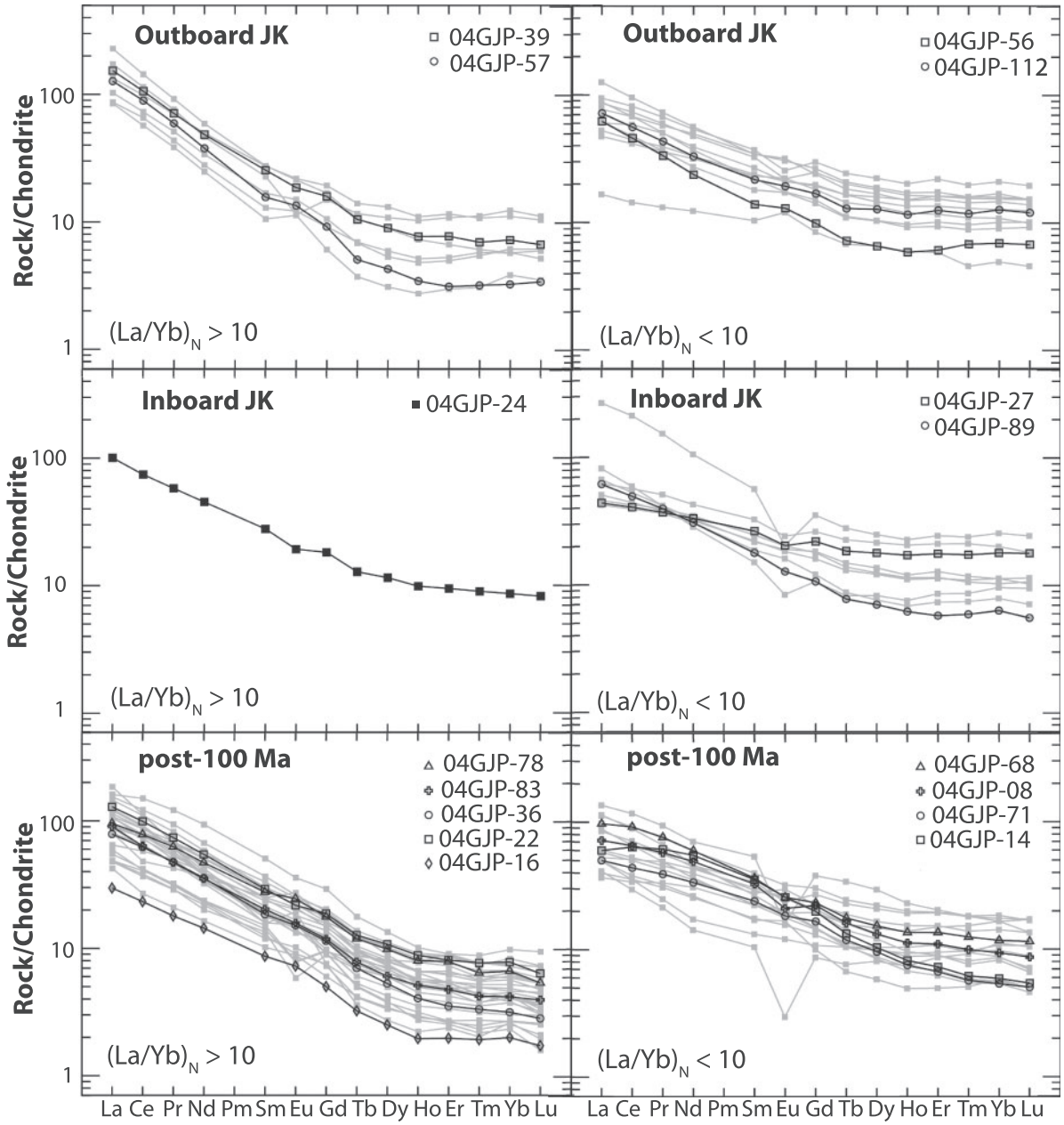

Fig. 7. Chondrite-normalized REE patterns for CMB samples of the three main arcs in this study. Chondrite-normalized La/Yb [$(La/Yb)_N$] of >10 shown at the left and <10 shown at the right. Whole sample suites are shown in gray; representative samples are shown in black.

the other samples lie close to Eu/Eu* = 1 (Fig. 6a). The partition coefficient of Eu^{2+} in plagioclase at depth in the crust is approximately two (Drake & Weill, 1975), exceeding partition coefficients for trivalent REE by nearly two orders of magnitude. Although differences in Eu partitioning exist for Ca-bearing mafic phases, they are small relative to the plagioclase effect (McKay, 1989). Redox conditions during magma genesis and transport should have maintained a high proportion of the Eu as Eu^{2+} (e.g. McKay, 1989). For the rocks of this study that do show anomalous Eu/Eu* (Fig. 6a), that effect could have been caused by plagioclase crystal fractionation, or by partial melting in the presence of plagioclase. The samples showing Eu anomalies constitute a group that shows up as anomalous on many trace element plots. From the majority of the CMB samples, we can conclude that most magmas have not equilibrated with large amounts of plagioclase, during either melting or crystal fractionation.

Original work on the granulite–eclogite transition in the presence of a basaltic melt, in which plagioclase disappears

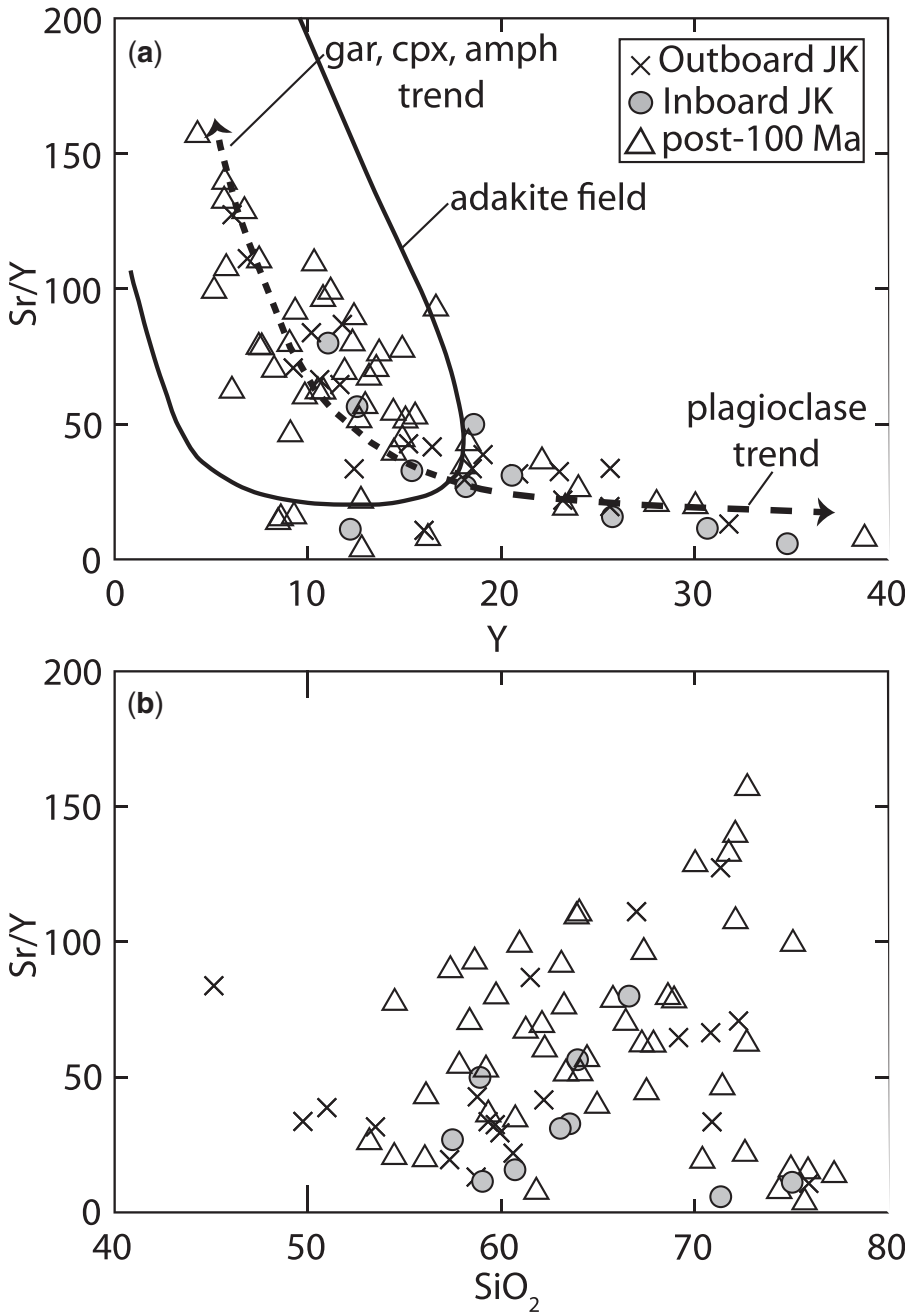

Fig. 8. (a) Sr/Y vs Y; (b) Sr/Y vs wt % SiO_2. In (a) continuous black line delimits the field of adakite-like rocks from Richards & Kerrich (2007). Dashed lines represent schematic trends for removal of magmas from different source mineralogies, or fractionating of phases, modified from Castillo *et al.* (1999).

from the rock assemblages, has suggested depths of around 60 km at 800°C for this set of reactions (Ito & Kennedy, 1971). Subsequent studies proposed the onset of eclogite-facies conditions at shallower depths, particularly if associated with melting of amphibolite (wet basalt). For this process, conditions above 1 GPa (equivalent to >35 km) and temperatures >900°C are suggested, above the disappearance of amphibole during dehydration melting (e.g. Wyllie, 1984; Wolf & Wyllie, 1994; Rapp & Watson, 1995). Calculations of the limit of plagioclase stability from thermodynamic data, using rock compositions expected beneath continental arc magmatic zones, have also placed this boundary at 40–45 km depth (e.g. Ducea, 2002; Saleeby *et al.*, 2003; Behn & Kelemen, 2006).

Table 3: Rare earth element (ppm) compositions of representative samples from this study

Sample	Group	La	Ce	Pr	Nd	Sm	Eu	Gd	Tb	Dy	Ho	Er	Tm	Yb	Lu	$(La/Yb)_N$	Eu/Eu*
04GJP-16	Ei	7·0	14·2	1·7	6·7	1·3	0·42	1·0	0·1	0·6	0·11	0·3	0·05	0·3	0·04	14·1	1·07
04GJP-14	CSZi	14·2	39·1	5·8	25·7	5·4	1·50	4·1	0·5	2·7	0·47	1·2	0·16	1·0	0·14	9·5	0·93
04GJP-22	ELK	22·7	44·3	5·1	18·6	3·3	0·97	2·8	0·3	1·8	0·30	0·8	0·11	0·7	0·09	21·3	0·95
04GJP-8	ELK	17·1	40·1	5·5	23·0	5·0	1·22	4·6	0·6	3·4	0·64	1·8	0·26	1·6	0·22	7·2	0·77
04GJP-83	EI	18·6	38·0	4·5	16·6	2·8	0·88	2·3	0·3	1·3	0·23	0·6	0·08	0·5	0·07	23·6	1·02
04GJP-71	EI	11·9	26·9	3·7	15·7	3·7	1·07	3·4	0·4	2·5	0·43	1·1	0·15	0·9	0·13	8·8	0·91
04GJP-36	EI	19·1	39·8	4·5	16·2	2·7	0·92	2·0	0·2	1·3	0·23	0·6	0·09	0·6	0·08	20·3	1·16
04GJP-78	ELK	34·7	67·8	7·8	27·3	4·6	1·38	3·8	0·5	2·7	0·50	1·4	0·19	1·4	0·19	16·6	0·98
04GJP-68	WMK	23·1	56·3	7·2	27·9	5·6	1·50	4·8	0·7	3·9	0·77	2·3	0·32	2·0	0·29	7·8	0·86
05MT-112	OJK-WMK	17·0	34·3	4·1	15·4	3·3	1·12	3·5	0·5	3·2	0·65	2·1	0·30	2·1	0·30	5·4	1·00
04GJP-39	OJK-eK	36·4	64·8	6·7	22·6	3·9	1·08	3·3	0·4	2·3	0·43	1·3	0·18	1·2	0·17	20·2	0·90
04GJP-89	IJK-eK	14·6	30·3	3·8	14·4	2·7	0·74	2·2	0·3	1·8	0·35	0·9	0·15	1·1	0·14	9·3	0·90
04GJP-56	OJK-eK	14·7	28·1	3·2	11·1	2·1	0·75	2·0	0·3	1·6	0·33	1·0	0·17	1·2	0·17	8·6	1·09
04GJP-57	OJK-IJ	30·1	54·7	5·6	17·6	2·4	0·78	1·9	0·2	1·1	0·19	0·5	0·08	0·5	0·09	37·2	1·08
04GJP-52	OJK-IJ	31·8	60·3	6·6	23·2	4·2	1·27	4·0	0·5	3·3	0·62	1·9	0·27	1·9	0·26	11·5	0·94
04GJP-24	IJK-mJ	23·8	45·5	5·5	21·1	4·3	1·12	3·8	0·5	2·9	0·56	1·6	0·23	1·5	0·21	11·0	0·84
04GJP-27	IJK-mJ	10·4	25·0	3·5	15·6	4·1	1·18	4·5	0·7	4·5	0·97	2·9	0·44	3·0	0·45	2·3	0·84

$(La/Yb)_N$ is chondrite-normalized ratio of La/Yb. $Eu/Eu^* = Eu_N/[0{\cdot}5(Sm_N + Gd_N)]$. The subscript N denotes that elements have been normalized relative to chondritic values (McDonough & Sun, 1995).

This depth appears to be approximately consistent with equilibration pressures calculated for granulite- versus eclogite-facies xenoliths from the Sierra Nevada continental arc (Ducea & Saleeby, 1996).

The transition from a plagioclase-bearing to a plagioclase-free assemblage in the root of the arc depends on a variety of factors such as pressure, temperature, and bulk composition; in general, it can be assumed that a depth range of 40–45 km below the arc surface is a good first-order approximation. Residual assemblages at greater depths would not consist exclusively of garnet and clinopyroxene, but could have various amounts of amphibole depending on the original proportion of this mineral in the assemblage.

The two constraints based on Eu and on plagioclase stability mean that it is very unlikely that most CMB granitoids have undergone significant magmatic processing (e.g. fractionation or assimilation) shallower than ~40 km, because melting or crystallization above 40 km would involve plagioclase as a residue mineral or a crystal fractionate. This depth limit is about 15 km greater than the depths indicated by the highest-pressure exposed metamorphic assemblages along our transects (Rusmore *et al.*, 2005). In general, the deepest exposures of Cordilleran batholiths in North America do not exceed 35 km (Barton *et al.*, 1988; Pickett & Saleeby, 1993; Ducea *et al.*, 2003).

K, Sm/Nd and Lu/Hf—limiting constraints for residual amphibole

Although Eu/Eu* provides some important constraints limiting the importance of plagioclase among the residual phases in the source of the CMB, and thus limiting melting and fractionation above ~35 km, it leaves unexplained the important question of why the rocks are overwhelmingly intermediate to felsic in composition. Orthopyroxene and clinopyroxene are clearly a major sink for Mg, Fe, Al and Ca; however, they both have silica concentrations in the range of ~50% SiO_2, making them poor candidates for driving the silica contents of magmas up towards 65%, if the starting magma is approximately mafic in composition. Garnet- and amphibole-group minerals differ from pyroxenes in having SiO_2 contents of 45% or less. Most arc root assemblages studied directly via xenoliths (Ducea & Saleeby, 1996; Lee *et al.*, 2001; Rodriguez-Vargas *et al.*, 2005) are amphibole–pyroxene–garnet rocks varying from amphibolites to pyroxenites, with or without garnet. Clearly, the minerals that are ultimately responsible for driving silica contents up in partially melted reservoirs (or magma chambers) located at depths below some

Table 4: Isotopic compositions of Rb and Sr for representative samples from this study

Sample	Group	Rb	Sr	$^{87}Rb/^{86}Sr$	$(^{87}Sr/^{86}Sr)_m$	$(^{87}Sr/^{86}Sr)_i$
04GJP-16	Ei	59·51	602·81	0·286	0·704408(14)	0·70420
04GJP-14	CSZi	37·34	785·28	0·138	0·703905(11)	0·70379
04GJP-22	ELK	47·29	782·78	0·175	0·704115(14)	0·70396
04GJP-8	ELK	51·04	614·80	0·240	0·703867(17)	0·70364
04GJP-83	EI	33·23	528·98	0·182	0·704126(15)	0·70392
04GJP-71	EI	45·37	589·96	0·222	0·704743(14)	0·70449
04GJP-36	EI	39·13	827·21	0·137	0·704422(15)	0·70425
04GJP-78	ELK	31·32	688·26	0·134	0·703712(49)	0·70353
04GJP-68	WMK	40·68	692·29	0·170	0·704911(14)	0·70468
05MT-112	OJK-WMK	35·41	503·78	0·203	0·704466(11)	0·70417
04GJP-39	OJK-eK	112·40	261·97	1·241	0·706074(14)	0·70405
04GJP-89	IJK-eK	32·47	730·76	0·129	0·703865(14)	0·70363
04GJP-56	OJK-eK	42·84	702·14	0·177	0·705014(16)	0·70466
04GJP-57	OJK-IJ	40·21	722·87	0·161	0·704886(14)	0·70456
04GJP-52	OJK-IJ	46·15	571·09	0·234	0·705417(17)	0·70493
04GJP-24	IJK-mJ	73·89	496·56	0·430	0·704083(18)	0·70313
04GJP-27	IJK-mJ	31·02	301·93	0·297	0·704180(14)	0·70342

Rb and Sr ppm determined by isotope dilution. $(^{87}Sr/^{86}Sr)_m$, measured ratio. Ratios normalized to $^{86}Sr/^{88}Sr = 0·1194$. The mean $^{87}Sr/^{86}Sr$ of NBS-987 runs (12) was 0·710229(11). $(^{87}Sr/^{86}Sr)_i$, initial ratio.

40 km are amphibole and/or garnet. The contribution of amphibole has to be of secondary importance compared with garnet, based on two geochemical arguments: the concentration of the major element K in melts and residues, and the positive correlation between Lu/Hf and Sm/Nd. These arguments are explained below.

The first argument is based on the overall mass balance of the major element potassium (expressed as its oxide K_2O) in arc magmas, mantle sources and residues. The positive correlation between silica and potassium in a Harker diagram (Fig. 4) requires by mass balance either that the residual mineral assemblage is very poor in K or that the average of the arc mass (melt plus restite or residue) had K_2O well above 1% at about 47–52% SiO_2. A reasonable average bulk K_2O content is about 0·2–0·4 wt %, consistent with the K_2O content of many mantle-derived basalts, including those at subduction margins (Otamendi *et al.*, 2009). However, amphiboles present as residual phases in arc xenoliths are relatively high in K_2O (~1%) (e.g. Ducea, 2002) similar to average hornblende in the CMB (our unpublished data), requiring that if amphibole is a significant residual phase, its K_2O content limits its abundance to less than 20% of the minerals present. There are xenolithic amphiboles from island arcs that have lower K_2O contents (less than 1%) (Conrad & Kay, 1984), but we consider that these are not typical of continental (Andean) arc environments.

The second line of argument against amphibole being the principal residual mineral is that there is a positive correlation between Lu/Hf and Sm/Nd for each magmatic group (Fig. 13), requiring that the residual mineral that causes the high Sm/Nd should also have a high Lu/Hf ratio. Whereas this does apply to garnet, it does not apply to amphibole, as observational data show that amphibole has much lower Lu/Hf than typical igneous whole-rocks (e.g. Anczkiewicz *et al.*, 2004), an observation also supported by partition coefficients between amphibole, garnet, and intermediate composition melts (Irving & Frey, 1978; Fujimaki *et al.*, 1984; Klein *et al.*, 1997). Dominant amphibole in the residue would have tended to cause an inverse correlation between Sm/Nd and Lu/Hf, rather than a positive one. We therefore argue that amphibole, although it may have been present, was not a principal component of the melting residues, or the main cause of higher silica in the magmas; we suggest that garnet is, by mass, the most important phase with this role. With a silica content of around 40 wt %, almandine–pyrope garnet can have a powerful effect on the SiO_2 content of magmas when it makes up a significant part of the residue assemblage.

SiO_2 vs HREE, Y and Sc—evidence for residual garnet

There is a group of trace elements, including Sr, U, Nb, Ta, Zr, Hf and the lighter REE La to Pr, which show no statistically significant correlation with SiO_2 (e.g. La and Nb in Fig. 5). Even if the rocks suspected from Eu/Eu*anomalies to have a shallower magma source or to have undergone some crystal fractionation at shallow crustal levels are disregarded, the correlation between La and SiO_2 is still poor. On the other hand, if SiO_2 is plotted against the heavier REE, from Gd to Lu, clear negative correlations are seen (Fig. 5). Samples that lie off these trends include some high-SiO_2 granitoids identified as potentially having shallower sources or to have undergone some crystal fractionation, and a gabbro and a mafic enclave mentioned above.

There is also a clear negative correlation between SiO_2 and Y and Sc (Fig. 5). The negative correlations between SiO_2 and Sc, Y, and Gd to Lu are observed for the Outboard JK arc, the Inboard JK arc, and the post-100 Ma arc. The common property that Sc, Y and HREE share is that they are partitioned strongly into garnet. With experimental and predicted partition coefficients between two and ~18, fairly small percentages of garnet will retain large proportions of available Y, Sc and HREE (Gromet & Silver, 1987; Klein *et al.*, 2000; van Westrenen *et al.*, 2000). It is not possible to distinguish between garnet that formed from the magmas as a crystal

Table 5: Isotopic compositions of Sm and Nd for representative samples from this study

Sample	Group	Sm	Nd	$^{147}Sm/^{144}Nd$	$(^{143}Nd/^{144}Nd)_m$	$(^{143}Nd/^{144}Nd)_i$	$\varepsilon_{Nd(i)}$	T(DM)
04GJP-16	Ei	1·38	7·17	0·1164	0·512848(11)	0·512808	4·6	334
04GJP-14	CSZi	4·95	24·43	0·1225	0·512898(06)	0·512851	5·6	275
04GJP-22	ELK	3·60	14·50	0·1500	0·512882(07)	0·512822	5·1	422
04GJP-8	ELK	5·13	23·57	0·1317	0·512896(10)	0·512837	5·6	309
04GJP-83	EI	2·26	11·00	0·1243	0·512899(10)	0·512833	5·8	279
04GJP-71	EI	3·30	13·69	0·1458	0·512837(10)	0·512758	4·4	493
04GJP-36	EI	2·85	17·01	0·1012	0·512792(10)	0·512731	4·1	364
04GJP-78	ELK	3·45	18·89	0·1103	0·512871(08)	0·512801	5·6	284
04GJP-68	WMK	5·47	27·98	0·1182	0·512689(16)	0·512614	2·0	583
05MT-112	OJK-WMK	2·91	13·77	0·1277	0·512826(08)	0·512740	4·6	413
04GJP-39	OJK-eK	4·22	22·67	0·1124	0·512817(08)	0·512731	4·7	366
04GJP-89	IJK-eK	2·58	13·43	0·1161	0·512893(08)	0·512794	6·3	266
04GJP-56	OJK-eK	2·07	11·79	0·1059	0·512690(09)	0·512591	2·7	517
04GJP-57	OJK-IJ	2·30	16·88	0·0823	0·512699(07)	0·512620	3·3	418
04GJP-52	OJK-IJ	3·65	17·98	0·1227	0·512715(15)	0·512595	2·9	567
04GJP-24	IJK-mJ	4·15	20·06	0·1249	0·512907(08)	0·512778	6·7	268
04GJP-27	IJK-mJ	3·62	14·20	0·1540	0·512954(17)	0·512770	7·2	278

Sm and Nd ppm determined by isotope dilution. $(^{143}Nd/^{144}Nd)_m$, measured ratio. Measured $^{143}Nd/^{144}Nd$ ratios normalized to $^{146}Nd/^{144}Nd = 0{\cdot}7219$. The mean $^{143}Nd/^{144}Nd$ of La Jolla Nd standard runs (18) was 0·511869(9). $(^{143}Nd/^{144}Nd)_i$, initial ratio. $\varepsilon_{Nd(i)} = [(^{143}Nd/^{144}Nd)sample/(^{143}Nd/^{144}Nd)CHUR(T) - 1] \times 10^4$; present-day value of $(^{143}Nd/^{144}Nd)CHUR = 0{\cdot}512630$. T(DM) based on the model of Bouvier *et al* (2008).

fractionate at a depth below plagioclase stability (>40 km) and garnet that was a residue phase during partial melting in the lower crust.

High Sr/Y—an additional effect of residual garnet

Another parameter that demonstrates the importance of a garnet-stable, plagioclase-free process of segregation of the magmas that crystallized close to the present-day surface of the CMB is Sr/Y. High Sr/Y ratios indicate a lack of a crystallizing plagioclase along the liquid line of descent, as plagioclase would have sequestered large amounts of Sr, whereas low Y concentrations implicate garnet as a retainer for this element (Fig. 8a). The fact that these high Sr/Y ratios are a characteristic of most intermediate to silicic CMB rocks (Fig. 8b) is a further indication that such 'adakite-like' signatures are the norm in our data, most of which cannot have been derived directly from melting peridotitic assemblages. Instead, they were probably derived from deep arc crustal domains where garnet was a significant component of the melting residue.

La/Yb and garnet-rich vs garnet-poor residues

The two differing types of REE patterns seen in Fig. 7 illustrate an important relationship in which the difference between the two types seems to have resulted largely from HREE depletion; this is supported by $(La/Sm)_N$ and $(Sm/Yb)_N$ ratios plotted in Fig. 6d. In Fig. 10 the chondrite-normalized La/Yb ratio is plotted against magmatic flux from Gehrels *et al.* (2009). Figure 10 shows that during the periods 200–160 Ma, 140–120 Ma, and 80–60 Ma, when average magmatic flux for all magma compositions (granitoids and more mafic rocks) was $\sim 15\,km^3\,Ma^{-1}km^{-1}$ or less, the exposed plutons have lower $(La/Yb)_N$, typically <10. In contrast, during the periods 160–140 Ma, 120–80 Ma, and 60–50 Ma, when the average magmatic flux was typically greater than $\sim 30\,km^3\,Ma^{-1}km^{-1}$, $(La/Yb)_N$ spans a greater range reaching values as high as 20–45. Based on these estimates, a magmatic flare-up corresponds to a flux at least twice as high as the baseline of $15\,km^3\,Ma^{-1}km^{-1}$.

Although other potential residual or fractionating phases such as amphibole or pyroxene do affect the REE (Schnetzler & Philpotts, 1970; Gromet & Silver, 1987; Blundy & Wood, 1994), significant HREE depletion is most probably due to removal of garnet, which has partition coefficients for the HREE of ~10 times those of amphibole or pyroxene (e.g. Klein *et al.*, 1997, 2000; Brophy, 2008). The overall concave-up REE patterns of some of our samples (Romick *et al.*, 1992) suggest that hornblende is also a participating phase in the residue.

Table 6: Major element (wt %) composition for anomalous samples of this study

Sample	Group	Rock type	Age (Ma)	SiO_2	TiO_2	Al_2O_3	Fe_2O_3*	MnO	MgO	CaO	Na_2O	K_2O	P_2O_5	LOI	Total	A/CNK	Mg#
04GJP-90	Ei	Tonalite	52	67·36	0·27	16·72	2·59	0·08	1·12	3·84	4·44	2·22	0·14	0·74	99·51	0·98	46
05MT-145	Ei	Granodiorite	52·3 ± 1·1	68·61	0·51	15·61	3·18	0·07	1·15	3·28	4·35	3·14	0·18	0·28	100·05	0·93	42
05MT-146	Ei	Granodiorite	52·4 ± 1·8	72·09	0·40	14·96	1·96	0·03	0·51	2·28	4·06	4·07	0·13	0·54	100·47	0·97	34
05MT-135	Ei	Tonalite	52·6 ± 1·4	71·75	0·24	15·66	2·20	0·03	0·64	3·79	4·44	1·32	0·10	0·47	100·15	0·98	37
04GJP-11	Ei	Granite	52·7 ± 1·5	74·96	0·09	14·06	0·86	0·08	0·23	0·78	4·25	3·78	0·09	0·62	99·82	1·13	35
04GJP-77	CSZi	Granodiorite	55·6 ± 0·9	70·02	0·41	15·98	2·55	0·03	0·77	3·18	4·64	1·73	0·16	0·31	99·78	1·03	37
05MT-137	Ei	Tonalite	61·1 ± 1·2	67·26	0·67	16·46	3·63	0·06	1·24	3·13	4·51	3·21	0·22	0·71	100·38	0·98	40
04GJP-6	ELK	Diorite[1]	74	61·81	0·79	17·62	6·38	0·31	1·90	2·33	5·71	2·50	0·29	0·53	100·15	1·08	37
04GJP-4	ELK	Granodiorite	74	77·20	0·09	13·23	0·84	0·05	0·13	0·67	4·53	3·58	0·04	0·27	100·62	1·05	24
05MT-105	ELK	Granodiorite	82·7 ± 1·6	72·59	0·30	14·98	2·29	0·07	1·38	1·20	3·83	3·75	0·07	0·90	100·44	1·19	54
04GJP-23	ELK	Granite	83·8 ± 2·8	75·85	0·06	14·38	0·65	0·10	0·14	0·88	4·35	3·91	0·04	0·41	100·77	1·10	30
05MT-101	ELK	Tonalite	85	74·36	0·04	15·38	0·28	0·01	0·07	1·14	4·15	5·39	0·04	0·39	100·84	1·04	32
05MT-97	ELK	Granodiorite	87	75·67	0·05	14·74	0·48	0·04	0·04	1·01	5·08	4·10	0·01	0·14	101·21	1·00	14
04GJP-32	EI	Qtz. diorite	92·1 ± 2·5	71·42	0·47	14·42	3·21	0·07	1·25	3·25	3·82	2·63	0·12	0·61	101·27	0·94	44
05MT-114	WMK	Qtz. diorite	94·3 ± 1·4	58·36	0·96	19·03	6·77	0·11	2·77	6·93	4·73	1·02	0·28	0·38	100·94	0·86	45
04GJP-40	WMK	Granodiorite	99·8 ± 2·3	64·95	0·38	16·72	5·18	0·15	1·81	5·41	3·53	1·56	0·16	0·57	100·43	0·93	41
05MT-116	OJK-WMK	Qtz. diorite	105	61·50	0·85	17·51	5·71	0·11	2·84	5·57	5·08	0·96	0·28	1·13	100·38	0·88	50
05MT-111	OJK-eK	Granodiorite	119·4 ± 4·3	75·89	0·21	13·24	1·66	0·05	0·33	1·16	3·59	4·78	0·05	0·26	100·94	1·00	28
05MT-121	OJK-lJ	Qtz. diorite	145	72·26	0·26	15·08	0·75	0·03	0·76	3·63	4·15	3·83	0·09	0·17	100·83	0·84	67
04GJP-50	OJK-lJ	Gabbro	152·7 ± 1·8	45·15	0·79	20·45	10·36	0·12	7·33	14·70	1·05	0·26	0·04	0·39	100·64	0·67	58
05MT-140	IJK-KC	Granodiorite	180·8 ± 2·6	75·03	0·20	13·77	1·85	0·03	0·40	1·39	3·99	3·80	0·06	1·72	100·51	1·03	30
05MT-138	IJK-KC	Granodiorite	210	71·34	0·44	14·54	2·94	0·08	0·69	2·07	4·25	3·73	0·12	1·27	100·18	0·97	32

[1]Mafic enclave sample.
Ei, Eocene intrusions; CSZi, Coast Shear Zone intrusions; ELK, Eastern late Cretaceous intrusions; EI, Ecstall intrusions; WMK, Western middle Cretaceous intrusions; OJK, Outboard Jurassic–Cretaceous; IJK, Inboard Jurassic–Cretaceous; eK, early Cretaceous; lJ, late Jurassic; KC, Kleanza Creek. Ages are U–Pb zircon ages as reported by Gehrels *et al.* (2009). Alumina Saturation Index, A/CNK, is the molar ratio of $Al_2O_3/(CaO + Na_2O + K_2O)$. Mg# = molecular MgO/(MgO + FeO); FeO calculated as $0·899 \times Fe_2O_3$*.

Experimental studies show that the garnet abundance in mafic lithologies increases over a pressure range of 1–2 GPa (~35 to ~70 km; Ito & Kennedy, 1971; Wolf & Wyllie, 1993). Thus our data are consistent with melting ranging from a depth at which garnet was low in abundance (perhaps around 35–40 km) to a greater depth (perhaps 45–50 km) where garnet could be one-third or more of the residual assemblage. We suggest that most magma sources were deeper than 40 km because even low-flux, low-$(La/Yb)_N$ magmas do not usually exhibit Eu anomalies.

Sr and Nd isotopic constraints

The Sr–Nd isotope data obtained as part of this study are in agreement with previous studies that suggested a dominantly 'juvenile' origin for the CMB rocks (Armstrong, 1988; Samson *et al.*, 1989; Samson *et al.*, 1991*a*; Cui & Russell, 1995; Friedman *et al.*, 1995), but with locally significant amounts of crustal material giving rise to ε_{Nd} values in the range from +2 down to slightly negative values (Samson *et al.*, 1991*a*; Patchett *et al.*, 1998). The oxygen isotope data of Wetmore & Ducea (2011) provide an important constraint in that although the plutons appear 'juvenile' with regard to Sr and Nd, their O isotope compositions are certainly not mantle-like and indicate the recycling of near-surface, crustal material. Both Hf-isotopic data for a subset of the samples presented in this study (Cecil *et al.*, 2011) and Sr–Nd isotope data from this study indicate an important crustal control on the isotopic composition of the CMB plutons.

The Sr–Nd isotopic differences between the plutons of the Outboard JK arc and plutons of the Inboard JK arc (Fig. 9) arc may reflect the isotopic characteristics of their host terranes. Only in the Outboard JK arc are isotopically continental-like rocks, the Banks Island assemblage (Boghossian & Gehrels, 2000; Gehrels & Boghossian,

Table 7: Trace element (ppm) compositions of anomalous samples of this study

Sample	Group	Sr	Rb	Ba	Th	U	Ta	Nb	Zr	Hf	Y	Co	Cr	Sc	Sr/Y
04GJP-90	Ei	1038	67	1802	3·0	2·6	0·7	6·8	97	2·8	11	6	19	23	96
05MT-145	Ei	721	74	1272	6·4	4·7	0·5	6·8	94	2·7	9	5	7	11	80
05MT-146	Ei	795	90	1791	9·3	2·4	0·3	4·7	112	2·8	6	2	15	6	139
05MT-135	Ei	752	24	819	6·1	0·6	0·2	3·4	215	6·1	6	4	5	19	132
04GJP-11	Ei	148	71	917	5·9	0·6	0·7	9·0	38	1·5	9	1	9	9	16
04GJP-77	CSZi	865	34	1086	2·9	0·4	0·2	4·6	145	4·0	7	4	6	19	129
05MT-137	Ei	653	68	1790	6·5	1·6	0·6	8·6	152	4·0	11	6	7	14	62
04GJP-6	ELK	297	131	399	9·2	3·9	1·1	21·9	123	3·7	39	10	12	18	8
04GJP-4	ELK	117	73	665	5·2	1·1	0·9	8·0	49	2·0	8	1	9	7	14
05MT-105	ELK	276	87	983	11·5	2·7	0·4	6·6	129	3·4	13	2	4	8	22
04GJP-23	ELK	131	79	1015	3·8	0·7	0·7	9·9	47	2·1	9	0	2	11	15
05MT-101	ELK	128	99	232	11·8	2·8	0·3	6·6	13	0·7	16	0	1	8	8
05MT-97	ELK	48	156	73	14·2	11·4	2·9	22·2	41	2·0	13	0	5	4	4
04GJP-32	EI	421	42	905	11·8	2·2	0·8	8·6	103	3·1	9	6	14	13	46
05MT-114	WMK	952	17	602	1·0	0·6	0·5	8·8	110	2·8	14	17	13	17	70
04GJP-40	WMK	570	35	608	1·9	1·0	0·6	5·9	70	2·2	14	10	17	18	39
05MT-116	OJK-WMK	1024	17	542	8·5	1·6	0·3	7·8	147	3·7	12	14	34	19	87
05MT-111	OJK-eK	173	112	1142	14·1	1·3	0·7	10·2	86	2·3	16	1	11	4	11
05MT-121	OJK-IJ	655	69	1903	4·3	1·8	0·7	10·0	128	3·3	9	2	9	11	71
04GJP-50	OJK-IJ	854	7	156	0·6	0·2	0·1	1·3	22	0·7	10	52	131	37	84
05MT-140	IJK-KC	137	103	822	9·5	3·0	0·5	4·9	125	3·1	12	2	8	7	11
05MT-138	IJK-KC	206	84	1130	13·5	2·3	0·7	8·2	162	4·5	35	3	4	14	6

2000), exposed at the surface. If equivalents of this assemblage were present and assimilated at the depth at which the arc magmas were generated, it could explain the apparently more crustal character of the Outboard JK arc compared with the Inboard JK arc (Fig. 9).

Plutons from the post-100 Ma arc exhibit fairly uniform variation in Sr–Nd isotopic space (Fig. 9). Initial ε_{Nd} values below +2 occur in the Douglas and Mathieson transects, whereas the Burke–Dean transect has no ε_{Nd} values lower than +2·8. This might suggest an influence of some older rocks present in the Central Gneiss Complex, which is exposed in the Douglas and Mathieson transects but not in the Burke–Dean transect (Fig. 1). However, we see no shift in ε_{Nd} values for plutonic rocks that are emplaced into, or lie close to the Central Gneiss Complex, so this effect cannot be documented.

Sr and Nd isotopic compositions show trends through time, as previously recognized elsewhere in the CMB (Armstrong, 1988; Ducea & Barton, 2007). When plotted against age and magmatic flux, initial $^{87}Sr/^{86}Sr$ (Fig. 11) and initial ε_{Nd} (Fig. 12) appear to be more sensitive to changes in magmatic flux than the more limited Hf isotopic dataset of Cecil *et al.* (2011). Despite a wide range of values, the most radiogenic Sr (higher $^{87}Sr/^{86}Sr$), and least radiogenic Nd (lower ε_{Nd}) occur during the late stages of periods, with high average magmatic flux at 160–140 Ma, 120–80 Ma, and 60–50 Ma. This phenomenon is best demonstrated between ~95–80 Ma and ~55–50 Ma, when $^{87}Sr/^{86}Sr$ reaches values >0·7045 and ε_{Nd} is < +3. During a cessation of magmatism at 140–120 Ma, and low-flux magmatism from 80 to 60 Ma, Sr and Nd lack excursions to less mantle-like values and typically have $^{87}Sr/^{86}Sr < 0{\cdot}7040$ and $\varepsilon_{Nd} > +4$.

The higher $^{87}Sr/^{86}Sr$ and lower ε_{Nd} during periods of high-flux magmatism indicate that a minor amount of older crustal material contributed to the magmas during those times, possibly incorporated into the lower crustal zone where the magmas were generated by tectonic underplating from the trench side or shortening from the back-arc side (Ducea & Barton, 2007). However, the 'older material' does not need to be ancient continental sediments or igneous rocks of Precambrian age. For the modest change in Sr and Nd isotopes during high-flux events, Paleozoic or even Mesozoic crustal contributions to the magma sources (earlier plutons of the CMB arc emplaced deep in the crust) are plausible.

Table 8: Rare earth element (ppm) composition for anomalous samples of this study

Sample	Group	La	Ce	Pr	Nd	Sm	Eu	Gd	Tb	Dy	Ho	Er	Tm	Yb	Lu	$(La/Yb)_N$	Eu/Eu*
04GJP-90	Ei	11·7	23·2	3·1	12·3	2·6	0·97	2·1	0·3	1·5	0·28	0·8	0·13	1·0	0·13	8·0	1·25
05MT-145	Ei	19·3	38·4	4·5	16·4	3·1	0·92	2·6	0·3	1·7	0·28	0·8	0·10	0·7	0·09	17·6	0·98
05MT-146	Ei	25·3	48·3	5·5	17·9	2·9	0·82	1·9	0·2	1·0	0·16	0·4	0·06	0·4	0·04	43·2	1·01
05MT-135	Ei	28·8	55·2	5·9	18·9	2·4	1·13	1·6	0·1	0·7	0·13	0·4	0·05	0·4	0·05	43·8	1·68
04GJP-11	Ei	13·1	25·9	3·0	10·9	2·2	0·46	2·0	0·3	1·8	0·33	0·9	0·13	0·8	0·11	10·7	0·66
04GJP-77	CSZi	20·9	38·8	4·5	15·1	2·4	0·90	1·9	0·2	1·0	0·18	0·4	0·06	0·4	0·05	32·8	1·23
05MT-137	Ei	36·7	75·0	9·0	31·5	5·6	1·52	4·0	0·5	2·3	0·36	0·9	0·11	0·7	0·08	38·3	0·93
04GJP-6	ELK	32·1	71·4	8·9	32·7	8·2	0·92	7·8	1·3	7·5	1·30	3·4	0·46	2·8	0·35	7·7	0·35
04GJP-4	ELK	11·5	23·5	2·8	9·4	2·1	0·34	1·8	0·3	1·5	0·28	0·8	0·12	0·7	0·10	11·1	0·52
05MT-105	ELK	29·4	56·7	5·8	17·8	2·9	0·77	2·3	0·3	2·1	0·44	1·5	0·22	1·7	0·24	12·0	0·88
04GJP-23	ELK	11·6	25·0	3·1	11·1	2·3	0·46	2·0	0·3	1·5	0·28	0·8	0·13	0·8	0·12	10·0	0·64
05MT-101	ELK	11·7	21·6	2·4	8·0	2·0	0·70	2·2	0·4	2·6	0·59	1·8	0·24	1·5	0·18	5·4	1·01
05MT-97	ELK	9·8	18·1	2·0	6·6	1·6	0·17	1·8	0·3	2·1	0·42	1·4	0·23	1·9	0·27	3·5	0·31
04GJP-32	EI	44·0	68·8	6·4	19·8	2·9	0·86	2·5	0·3	1·6	0·31	0·9	0·13	0·9	0·13	33·7	0·94
05MT-114	WMK	19·2	29·6	4·1	17·0	3·8	1·59	3·4	0·5	2·6	0·47	1·3	0·17	1·1	0·15	11·4	1·33
04GJP-40	WMK	9·4	21·7	2·9	11·9	2·7	0·90	2·7	0·4	2·5	0·53	1·6	0·25	1·8	0·27	3·5	1·02
05MT-116	OJK-WMK	54·1	87·7	8·7	27·5	4·2	1·23	3·5	0·4	2·2	0·41	1·1	0·15	1·0	0·13	37·7	0·96
05MT-111	OJK-eK	40·9	69·7	7·2	21·6	3·5	0·66	3·1	0·4	2·7	0·58	1·8	0·28	2·1	0·28	13·3	0·61
05MT-121	OJK-IJ	20·6	40·1	4·1	13·0	2·0	0·70	1·9	0·3	1·5	0·29	0·9	0·15	1·0	0·15	14·4	1·10
04GJP-50	OJK-IJ	3·9	8·8	1·3	5·8	1·6	0·69	1·7	0·3	1·7	0·34	1·0	0·12	0·8	0·12	3·2	1·28
05MT-140	IJK-KC	19·5	36·6	4·0	13·5	2·3	0·49	2·2	0·3	2·1	0·43	1·4	0·22	1·6	0·24	8·1	0·65
05MT-138	IJK-KC	63·8	131·0	14·7	49·7	8·7	1·19	7·3	1·1	6·3	1·29	4·0	0·61	4·4	0·62	10·0	0·45

$(La/Yb)_N$ = chondrite-normalized ratio of La/Yb. $Eu/Eu^* = Eu_N/[0{\cdot}5(Sm_N + Gd_N)]$. The subscript N denotes that elements have been normalized relative to chondritic values (McDonough & Sun, 1995).

Implications for magma sources and magmatic processes

One implication of the negative correlations between Sc, Y, Gd, and Yb and SiO_2 (Fig. 5) and the lack of Eu anomalies in most CMB granitoids (Fig. 6a) is that the source region of the CMB magmas must have been close to that of the lower depth limit of plagioclase stability, and probably deeper into the field of garnet stability. Seven of the rocks with ~75% SiO_2 do have negative Eu anomalies (Fig. 6a), showing a probable change of composition by crystal fractionation (or a shallower plagioclase-stable source). However, there are 12 samples with 70–75% SiO_2 that do not have Eu anomalies; of these 10 appear to have equilibrated with garnet and have $(La/Yb)_N$ between 10 and 43. Two high-silica samples with no Eu anomaly and $(La/Yb)_N$ of ~6 do not appear to have equilibrated with garnet.

Experiments that produce intermediate to silicic melts from plausible lower crustal bulk compositions at pressures >1 GPa have shown that silica content rises with more garnet in the residue and with lower degrees of melting (Wolf & Wyllie, 1994; Rapp & Watson, 1995). Clinopyroxenes expected in eclogitic assemblages have SiO_2 contents of around 50 wt %, but because almandine garnets have 38–41% SiO_2, residual garnet may cause enrichment of SiO_2 in magmas when it is a significant residue component (see Wolf & Wyllie, 1994; Rapp & Watson, 1995).

Variations in the abundance of garnet in the source or as a fractionating phase are the most likely cause of variations in the HREE in chondrite-normalized REE patterns (Kay *et al.*, 2005; Fig. 7). In contrast to the Peninsular Ranges Batholith, these patterns do not correlate geographically (e.g. Gromet & Silver, 1987), but rather scatter over different ranges especially during periods of higher magmatic flux (Fig. 10). This may indicate a fluctuation in the depth range of the magma sources, which were overall deeper during periods of higher magmatic flux, and resulted in higher garnet growth in the residue. There simply is no space for the majority of the residual masses to be located at shallow crustal levels, as the CMB itself is exposed to an average of 20 km paleodepth (Gehrels *et al.*, 2009).

Table 9: Isotopic composition of Rb and Sr in anomalous samples of this study

Sample	Group	Rb	Sr	$^{87}Rb/^{86}Sr$	$(^{87}Sr/^{86}Sr)_m$	$(^{87}Sr/^{86}Sr)_i$
04GJP-90	Ei	13·04	937·85	0·040	0·703847(15)	0·70382
05MT-145	Ei	52·45	676·47	0·224	0·705898(14)	0·70573
05MT-146	Ei	72·1	746·29	0·279	0·706117(14)	0·70591
05MT-135	Ei	65·57	627·21	0·302	0·706993(16)	0·70677
04GJP-11	Ei	72·82	146·65	1·436	0·705224(38)	0·70416
04GJP-77	CSZi	28·86	744·04	0·112	0·704522(27)	0·70443
05MT-137	Ei	66·06	639·34	0·299	0·705472(13)	0·70522
04GJP-6	ELK	n.d.	n.d.	n.d.	n.d.	n.d.
04GJP-4	ELK	61·10	109·40	1·615	0·705430(13)	0·70376
05MT-105	ELK	82·7	258·79	0·925	0·710220(14)	0·70915
04GJP-23	ELK	79·18	127·84	1·791	0·705530(14)	0·70343
05MT-101	ELK	93·68	114·8	2·361	0·707787(16)	0·70498
05MT-97	ELK	n.d.	n.d.	n.d.	n.d.	n.d.
04GJP-32	EI	42·77	405·46	0·305	0·704743(14)	0·70435
05MT-114	WMK	17·23	934·71	0·053	0·704325(13)	0·70425
04GJP-40	WMK	26·84	382·86	0·203	0·704175(14)	0·70389
05MT-116	OJK-WMK	16·71	996·93	0·049	0·704455(14)	0·70438
05MT-111	OJK-eK	110·49	165·58	1·930	0·707831(17)	0·70460
05MT-121	OJK-IJ	21·63	719·99	0·087	0·704233(14)	0·70406
04GJP-50	OJK-IJ	6·63	776·26	0·025	0·706189(13)	0·70614
05MT-140	IJK-KC	83·54	132·14	1·829	0·708408(16)	0·70377
05MT-138	IJK-KC	71·5	196·33	1·054	0·707481(14)	0·70438

Rb and Sr ppm determined by isotope dilution. $(^{87}Sr/^{86}Sr)_m$, measured ratio. Ratios normalized to $^{86}Sr/^{88}Sr = 0·1194$. The mean $^{87}Sr/^{86}Sr$ of NBS-987 runs (12) was 0·710229(11). $(^{87}Sr/^{86}Sr)_i$, initial ratio. n.d., not determined.

An important facet of the developing knowledge of the Canadian Cordillera is that seismic constraints do not provide any evidence for residues that are required to have formed at the base of the crust (Calkins *et al.*, 2010). Although ultramafic residues are difficult to distinguish seismically from peridotite, it appears that these assemblages, whenever formed, have been recycled into the mantle (Mahoney *et al.*, 2009), as first suggested in a pioneering paper that studied primarily the Aleutian Arc but also identified the CMB as a possible analogue example (Kay & Kay, 1988, fig. 5). A recent isotopic study of small-volume, high-MgO primitive basalts (Manthei *et al.*, 2010) from the same geographical area as this study shows that a major isotopic transition from CMB-like isotopic ratios to significantly more depleted Sr and Nd isotopic ratios took place during the mid-Miocene, thus providing some constraints on the timing of regional lithospheric thinning.

POSSIBLE MODELS FOR CMB PETROGENESIS

Petrological and geochemical factors

The template of mantle melting processes in the presence of slab-derived fluids and melt migration in subduction zones is provided by numerous studies of island arc magmas and related experimental work (e.g. Davies & Stevenson, 1992; Stolper & Newman, 1994; Schmidt & Poli, 1998; Grove *et al.*, 2003; Jagoutz *et al.*, 2011). It is clear, however, that mature, long-lived arcs built on a continental upper plate are subject to additional magmatic and structural complexities that are ultimately responsible for significantly greater crustal thickness, petrographic diversity, and intermediate to felsic magma compositions (e.g. Gromet & Silver, 1987; Hildreth & Moorbath, 1988).

The geochemical characteristics of the CMB detailed in this study impose several requirements on models for batholith generation, as follows: (1) most magma processing, whether melting, crystal accumulation or assimilation, must have taken place deeper than the 35–40 km limit of plagioclase stability; (2) garnet was a residual mineral during melting for many of the magmas, becoming an increasing component of the residue for magmas generated when the arc magma flux was high; (3) the importance of residual garnet also suggests that most melting took place below 35 km depth; (4) contributions to magma sources from recycled ancient continental materials were very small; (5) during high magma-flux periods there were modest increases in the amount of recycled continental materials that became involved in magma generation, although the age and origin of the recycled components in the magmas are unconstrained.

A mechanism that has long been invoked to explain the generation of large volumes of granitoid magma by crustal melting is that the magmas form as water-bearing minerals are dehydrated (e.g. Wyllie, 1984; Vielzeuf & Holloway, 1988); the availability of water can lower the melting temperature of the source rocks by several hundred degrees and allows significant volumes of magma to be produced. Whatever the source of the CMB magmas, it seems very likely that large magma volumes were produced contemporaneously with dehydration reactions, accompanied by added heat and mass from mantle-wedge contributions (hydrous basalts), otherwise the heat required would have been far greater.

Crustal rocks under granulite-facies conditions could satisfy the garnet constraint, and in many other orogenic belts, granite genesis can be directly observed to occur as amphibolite-facies metamorphic assemblages are transformed to granulite, with liberation of water from micas and amphiboles (e.g. Solar & Brown, 2001). Granitoid genesis under these general conditions from deep crustal metamorphic rocks has been invoked in many orogenic belts (e.g. Frost & O'Nions, 1985; Frost & Frost, 1987; Brown,

Table 10: Isotopic compositions of Sm and Nd in anomalous samples of this study

Sample	Group	Sm	Nd	$^{147}Sm/^{144}Nd$	$(^{143}Nd/^{144}Nd)_m$	$(^{143}Nd/^{144}Nd)_i$	$\varepsilon_{Nd(i)}$	T(DM)
04GJP-90	Ei	2·10	9·76	0·1302	0·512958(09)	0·512914	6·7	198
05MT-145	Ei	3·23	17·06	0·1145	0·512582(07)	0·512543	−0·5	721
05MT-146	Ei	2·80	18·18	0·0932	0·512491(07)	0·512459	−2·2	708
05MT-135	Ei	2·11	13·39	0·0954	0·512725(07)	0·512692	2·4	429
04GJP-11	Ei	1·60	6·95	0·1394	0·512956(13)	0·512908	6·6	224
04GJP-77	CSZi	1·91	12·43	0·0931	0·512834(10)	0·512800	4·6	290
05MT-137	Ei	6·27	35·57	0·1065	0·512646(08)	0·512603	0·9	580
04GJP-6	ELK	n.d.	n.d.	n.d.	n.d.	n.d.	n.d.	n.d.
04GJP-4	ELK	2·27	10·62	0·1291	0·512919(07)	0·512857	6·1	260
05MT-105	ELK	2·77	17·55	0·0955	0·512406(08)	0·512354	−3·5	828
04GJP-23	ELK	2·45	11·71	0·1266	0·512934(06)	0·512865	6·5	229
05MT-101	ELK	1·28	5·33	0·1453	0·512741(13)	0·512660	2·6	691
05MT-97	ELK	1·38	6·36	0·1310	0·512761(15)	0·512686	3·1	541
04GJP-32	EI	2·95	16·10	0·1107	0·512787(09)	0·512720	3·9	403
05MT-114	WMK	3·46	16·19	0·1291	0·512788(10)	0·512708	3·7	485
04GJP-40	WMK	2·30	9·07	0·1534	0·512900(07)	0·512800	5·7	403
05MT-116	OJK-WMK	4·00	21·46	0·1127	0·512742(07)	0·512665	3·2	475
05MT-111	OJK-eK	3·56	22·35	0·0962	0·512634(09)	0·512559	1·5	547
05MT-121	OJK-IJ	2·09	13·16	0·0958	0·512723(08)	0·512632	3·5	434
04GJP-50	OJK-IJ	1·48	5·47	0·1633	0·512519(11)	0·512356	−1·7	1574
05MT-140	IJK-KC	1·91	10·23	0·1131	0·512831(08)	0·512697	5·7	349
05MT-138	IJK-KC	6·76	37·10	0·1101	0·512796(06)	0·512645	5·4	388

Sm and Nd ppm determined by isotope dilution. $(^{143}Nd/^{144}Nd)_m$, measured ratio. Measured $^{143}Nd/^{144}Nd$ ratios normalized to $^{146}Nd/^{144}Nd = 0{\cdot}7219$. The mean $^{143}Nd/^{144}Nd$ of La Jolla Nd standard runs (18) was 0·511869(9). $(^{143}Nd/^{144}Nd)_i$, initial ratio. $\varepsilon_{Nd(i)} = [(^{143}Nd/^{144}Nd)sample/(^{143}Nd/^{144}Nd)CHUR(T) - 1] \times 10^4$; present-day value of $(^{143}Nd/^{144}Nd)CHUR = 0{\cdot}512638$. T(DM) based on the model of Bouvier *et al.* (2008). n.d., not determined.

2001). Most granulite-facies crustal lithologies contain abundant plagioclase, which would cause Eu anomalies in any magma separated from them. For the small number of CMB plutons that do exhibit Eu anomalies (Fig. 3), generation by partial melting of granulite-facies rocks is possible (alternatively the Eu anomalies could be generated by crystal fractionation). For the vast majority of CMB plutons, however, the lack of Eu anomalies argues against granulite sources. This interpretation is consistent with trace element evidence for the greatest majority of large batholiths in North America (e.g. Gromet & Silver, 1987; Ducea, 2002), and for stratovolcanoes and related volcanism in the modern Andes (Mamani *et al.*, 2010).

Considering the depth limits from plagioclase, and the domination of trace element fractionation by garnet, it is more likely that the water that became available for lowering melting temperatures would have been generated by the transformation of amphibolite to eclogite, rather than granulite, in the presence of a hydrous intermediate calc-alkaline melt. Under these conditions, garnet becomes abundant in the residues as melts are produced, but plagioclase is not stable, and disappears as the reactions or melting proceeds. These melting concepts, developed from wet basalt dehydration melting experimental studies (Rapp, 1995; Rapp & Watson, 1995), and also from studies of continental arcs (rather than orogenic belts made of metamorphosed sedimentary rocks) represent a different paradigm for granitoid genesis, one that focuses attention on the formation of juvenile continental crust (e.g. Kay & Kay, 1991, 1993; Ducea, 2001; Jull & Kelemen, 2001; Saleeby *et al.*, 2003).

There are two possible models for the generation of the CMB magmas that satisfy the available constraints: melting of the subducting mafic slab plus sediments (Castro *et al.*, 2010), and melting of deep masses of igneous or sedimentary rocks emplaced onto or into the base of the crust by tectonic underplating (Ducea *et al.*, 2009) and retro-arc crustal thickening (DeCelles *et al.*, 2009). We explore each of these.

Slab melting has been identified as a likely process at some present-day subduction zones (e.g. Kay, 1978; Defant & Drummond, 1990; Kelemen *et al.*, 2003), and has been

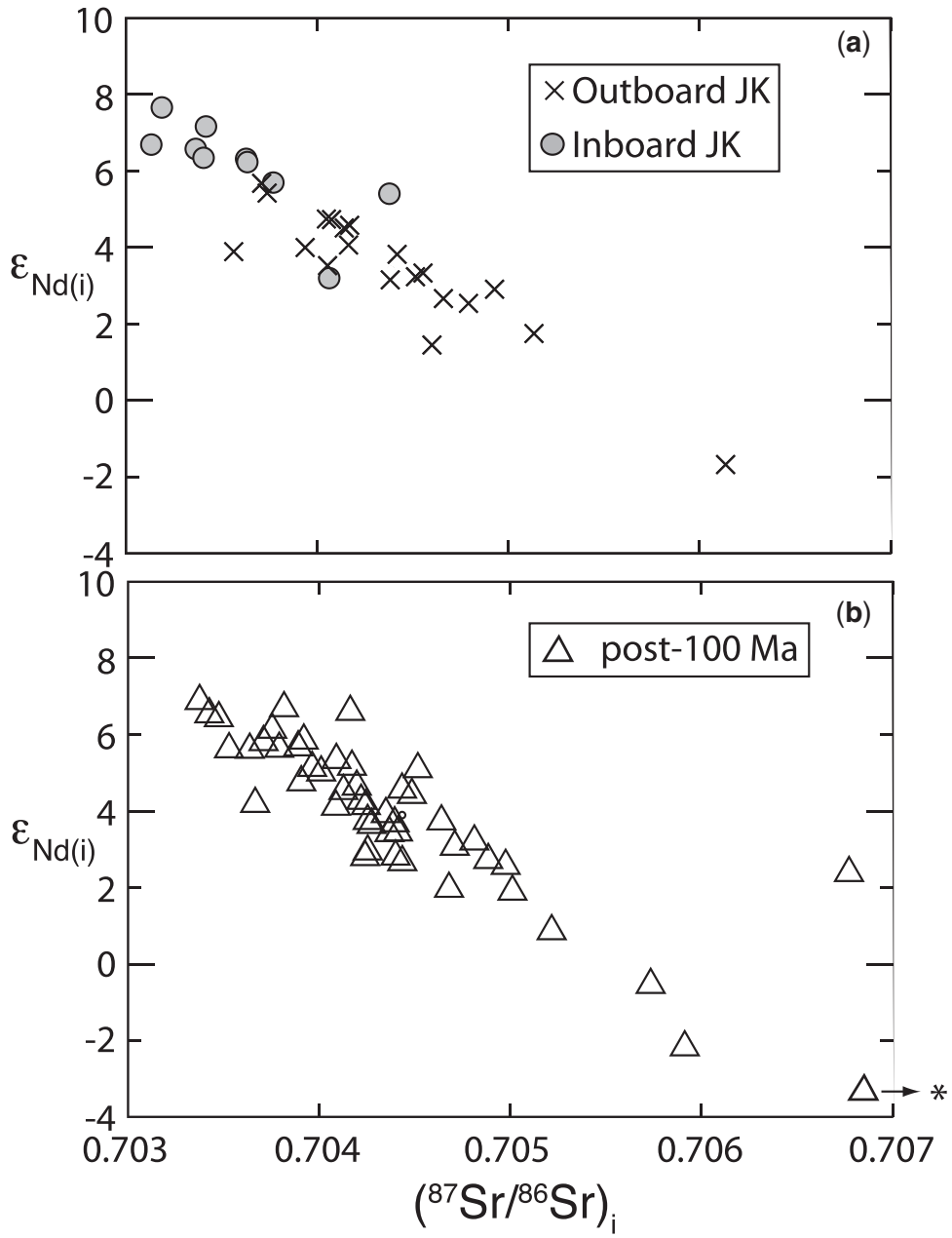

Fig. 9. Nd and Sr isotopic variations for CMB samples: (a) Outboard JK arc and Inboard JK arc; (b) post-100 Ma arc.

repeatedly invoked to explain Archean trondhjemites, tonalities and granodiorites with steeply sloping REE patterns (e.g. Drummond & Defant, 1990; Martin, 1993; McCulloch, 1993). Because the upper layer of the subducting slab is basaltic rock, which transforms to eclogite during subduction, there is a ready source of water from dehydration reactions, as garnet and pyroxene become stable, and plagioclase disappears. Slab melting could explain CMB magma generation on the basis of our data; however, there are reasons why it may be an unlikely process.

First, it is highly unlikely that large volumes of magma with 65–70 wt % SiO_2 [in excess of (4–5) $\times$ 10^6 km^3 in total] could be formed by long-term slab melting. Slab melting takes place in special circumstances, requiring an unusually hot slab with the trench close to the ridge (Peacock, 1990, 1993; Hacker *et al.*, 2003) or very slow relative plate convergence, which is not supported in our study area by plate reconstructions (Engebretson *et al.*, 1985). In addition, oceanic slab-derived melts would tend to show positive correlations in $^{87}Sr/^{86}Sr$ – $^{143}Nd/^{144}Nd$

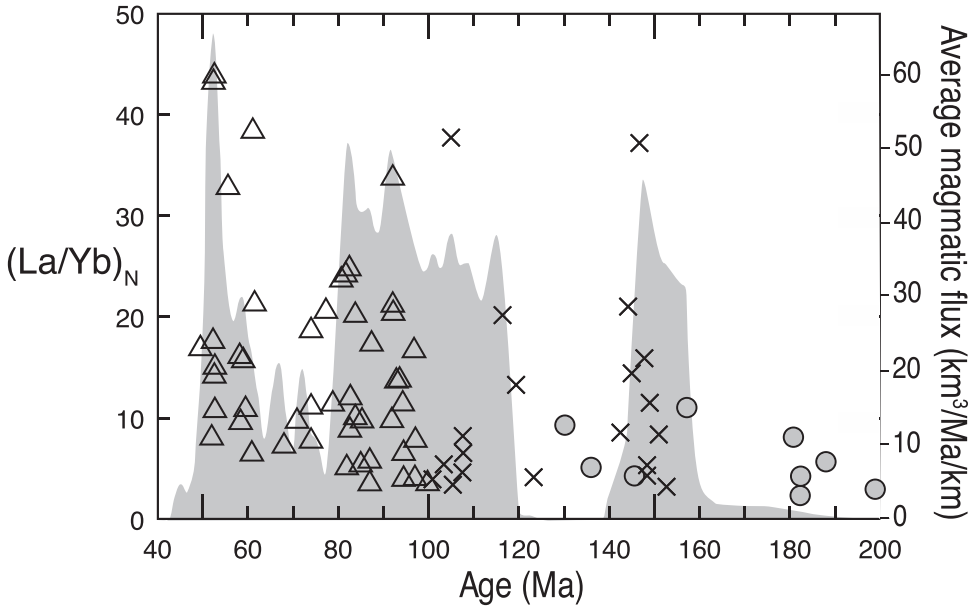

Fig. 10. $(La/Yb)_N$ vs age (Ma) for CMB samples. The left vertical axis is scaled for $(La/Yb)_N$, and the right axis shows variations in average magmatic flux (graphed as grey background) from Gehrels *et al.* (2009). Symbols as in Fig. 9.

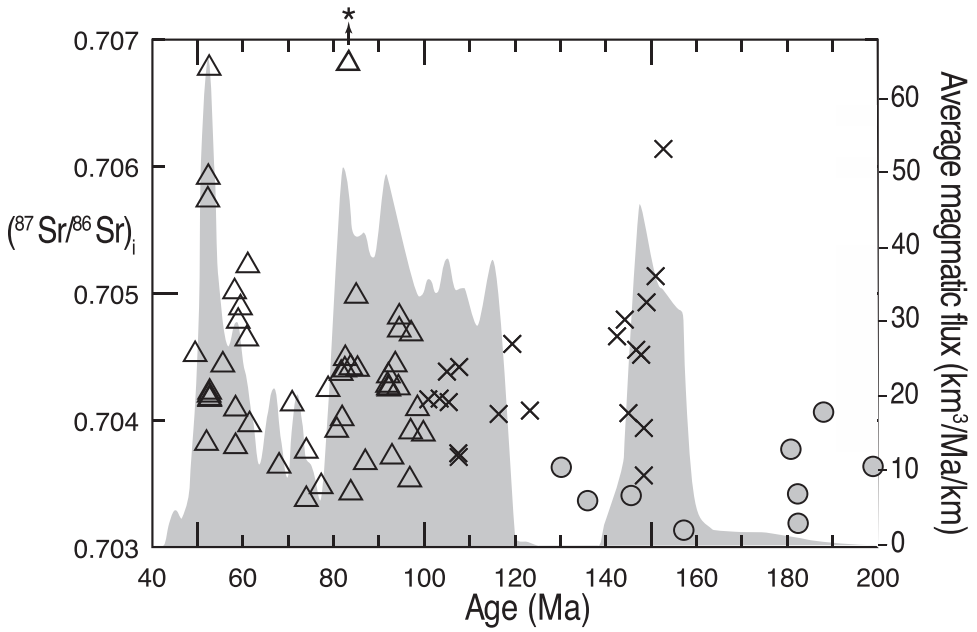

Fig. 11. Initial $^{87}Sr/^{86}Sr$ for CMB samples vs age (Ma). The left vertical axis is scaled for initial $^{87}Sr/^{86}Sr$, and the right axis shows variations in magmatic flux (graphed as grey background) from Gehrels *et al.* (2009). Symbols as in Fig. 9.

isotopic diagrams as $^{87}Sr/^{86}Sr$ would be increased owing to interaction of the oceanic crust with seawater, whereas $^{143}Nd/^{144}Nd$ would be unaffected by seawater (Staudigel *et al.*, 1995). We do not observe any effect predicted by a source with such characteristics. Furthermore, the $^{143}Nd/^{144}Nd$ record, although primitive and typical for the mantle array, suggests that few of the source rocks could have been ocean crust derived from a depleted MORB mantle (see Stern & Kilian, 1996), as required by the slab and sediment models (e.g. Castro *et al.*, 2010).

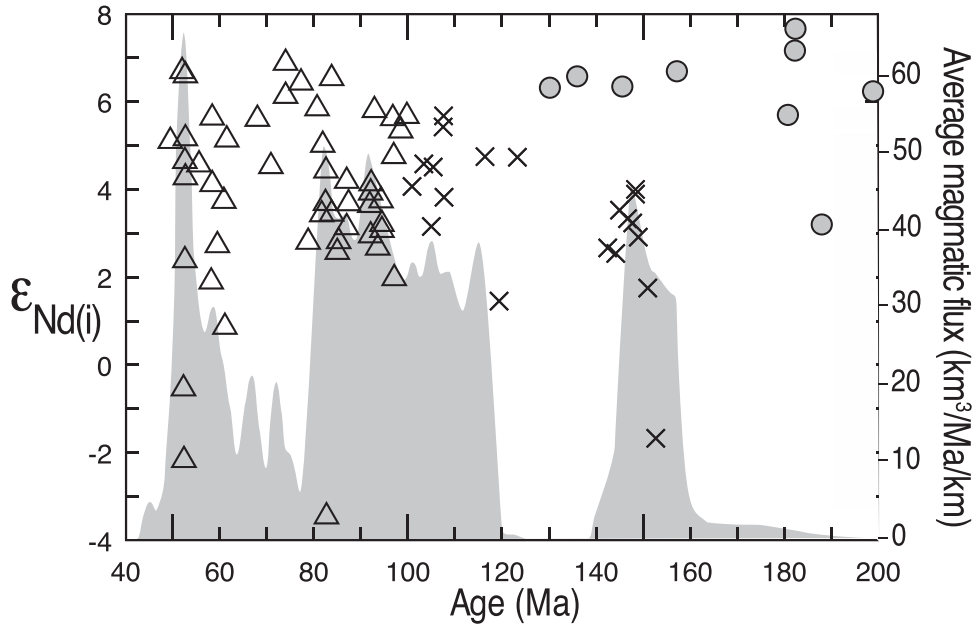

Fig. 12. Initial ε_{Nd} for CMB samples vs age (Ma). The left vertical axis is scaled for initial ε_{Nd}, and the right axis shows variations in magmatic flux (graphed as grey background) from Gehrels *et al.* (2009). Symbols as in Fig. 9.

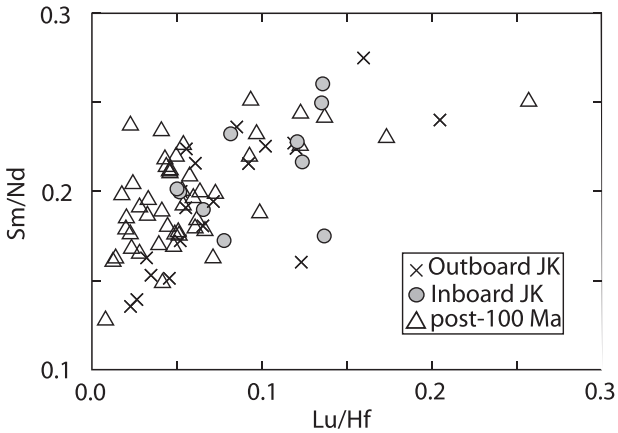

Fig. 13. Variation of Lu/Hf with Sm/Nd; symbols as in Fig. 9. (See text for further details.)

Tectonic underplating from the trench side is an ephemeral process in which the mantle wedge is not present between the upper and lower plates significantly inland from the trench, and allows wedge sediments and sometimes parts of the forearc to be tectonically accreted to the bottom of the upper plate (Ducea *et al.*, 2009). The normal consequence of this extreme case of shallow subduction is that the arc migrates suddenly inboard (and the earlier site of magmatism freezes). Although there is evidence for such processes in the North American Cordillera (e.g. Saleeby, 2003), the fact that the CMB magmatism did not suddenly jump inboard by ~100 km or more argues against that mechanism.

An overthickened crust of material derived from the foreland (back-arc) side has been viewed as a potential site for granitoid generation in mature continental arcs (e.g. Patiño-Douce *et al.*, 1990; Ducea, 2001; Mantle & Collins, 2008; DeCelles *et al.*, 2009). Magma generation would take place at lower crustal depths in thickened crust, and dense ultramafic residues, rich in garnet and pyroxene, but not in olivine, could detach and sink into the convecting mantle (Gromet & Silver, 1987; Kay & Kay, 1993; Saleeby *et al.*, 2003). Heating of the lower crust is significantly aided by emplacement of primitive basaltic magmas from the mantle wedge at a typical rate of 0·2 km thickness Ma^{-1} (Reymer & Schubert, 1984; Stern, 2011). This rate would correspond to a mafic magma addition rate of about 10 $km^3\,km^{-1}\,Ma^{-1}$ in Figs 10–12, for a 100 km width of the arc. Because most CMB magmas display the fingerprint of residual garnet, and at the same time very small to no effects from residual plagioclase, we propose that this process was significant and perhaps repeated during the long-term evolution of the arc. Evidence for extreme shortening of the foreland is plentiful in the region as the orogen terminates eastward with long-lived fold and thrust belts (the Canadian Rockies), although the magnitude and timing of shortening are yet to be quantified in the immediate vicinity of the arc.

Magmatic episodes in the CMB

Armstrong (1988), Ducea & Barton (2007), and Gehrels *et al.* (2009) showed that the CMB is characterized by alternating high and low magma flux episodes throughout its evolution. These episodes are long-lived, 20–40 Myr on average. The fluxes used in this study are from Gehrels *et al.* (2009) and represent only the intermediate contributions to the arc mass. Deeper, mafic plutons and residual masses are expected to be at least as voluminous (up to three times; Ducea, 2002). In addition, there is a volcanic flux, which is impossible to quantify for most extinct North American arcs, but is considered to be significantly less, by a factor of 5–10, than the intrusive fluxes.

High $(La/Yb)_N$, suggesting the influence of garnet on magma genesis, is coupled with high $^{87}Sr/^{86}Sr$ and low ε_{Nd} values during all periods of high magmatic flux (Figs 10–12). The periods at 160–140, 120–80 and 60–50 Ma do not appear to be geochemically distinct in terms of gross magma compositions. Considered as a whole, our data share many features with those of Andean rocks (Haschke *et al.*, 2002; Kay *et al.*, 2010; Mamani *et al.*, 2010). However, the tectonic history of the Canadian Cordillera, as documented in the exposures at the present surface, should constrain the nature of any crustal or lithospheric thickening events.

In the Jurassic to earliest Cretaceous, any interpretations are hampered by the fact that two distinct arc segments are present, and that all the higher-flux magmatism is associated with the Outboard JK arc (Gehrels *et al.*, 2009). The Outboard JK arc displays high $(La/Yb)_N$ coupled with high $^{87}Sr/^{86}Sr$ and low ε_{Nd} values. A complication, however, is that the plutons in the Ourboard JK arc also have lithologies with ancient continental signatures within their country rocks at the present erosion level, and it is not clear if this special assemblage is also present at the depth of magma genesis. The Inboard JK arc, sited on the Stikine terrane, has much lower flux, and somewhat different geochemical signatures. No pluton has $(La/Yb)_N$ higher than ~11, and one important suite of plutons has negative Eu anomalies. These features suggest shallower magma genesis under the Stikine terrane.

It is in the late Cretaceous that geological evidence (e.g. Crawford *et al.*, 1987; Rubin *et al.*, 1990) and reconstructed plate motions (Engebretson *et al.*, 1985) most clearly indicate contraction and thickening. This contraction was associated with the accretion of the Insular superterrane (Alexander+Wrangellia terranes), the timing of initiation of which is uncertain, but which was definitely generating features associated with plate collision by mid-Cretaceous times (Monger *et al.*, 1994). Consensus exists for thickening associated with this compression at least during the period 100–80 Ma (Crawford *et al.*, 1987; Rubin *et al.*, 1990; Rusmore & Woodsworth, 1991; Hollister & Andronicos, 2006). It is at or near the base of this overthickened orogenic wedge that we envisage a long-lived partial melting zone, where broadly mafic crustal lithologies generated granitoids with SiO_2 up to 65% and sometimes higher, leaving eclogitic or garnet pyroxenitic residues. This is similar to the MASH-zone concept of Hildreth & Moorbath (1988).

The high-flux magmatic event from about 60 to 50 Ma is less straightforward to explain. The CMB arc was undergoing oblique convergence during the period before 67 Ma, but this changed to arc-parallel motion by the time CMB magmatism ended (Crawford *et al.*, 1999). Thrusting continued until ~55 Ma, but this was replaced by an extensional regime from 55 to 50 Ma (Crawford *et al.*, 1987; Rubin *et al.*, 1990; Rusmore & Woodsworth, 1991; Rusmore *et al.*, 2001; Hollister & Andronicos, 2006). The general impression is that of a progressive shutdown of orogenesis starting around 60 Ma. In these circumstances, we conclude that granitoid magmas may have been produced at >40 km depth during earlier thickening, probably continued to be produced in the thickened crust in the earlier stages of extension, but were often emplaced into mid- and upper-crustal assemblages as they were undergoing extension. Another factor is that an oceanic spreading center was probably subducted beneath the CMB during the 60–50 Ma interval (Haeussler *et al.*, 2003), and this may have promoted melting of overlying crustal assemblages.

Comparisons with other arcs

The CMB is the largest coastal batholith in North America. Together with the Peninsular Ranges, Sierra Nevada, Idaho and Cascades batholiths, it forms a more or less continuous track of plutonic masses parallel to the trench separating North America from the Pacific. These batholiths represent the intrusive equivalent of the modern frontal arc of the Andes, which is represented by large andesitic to dacitic stratovolcanoes, and the giant dacitic ignimbrites of the Altuplano–Puna. Integrating these two 'views', the surficial one provided by the modern Andean volcanic arc and the deeper one of the eroded North American arcs, is essential for a better understanding of arc magmatism. The findings of this study are similar to recent results and compilations for other North American batholiths in that high magmatic flux events (1) are episodic, (2) are characterized by isotopic excursions to more crustal-like compositions, and (3) tend to form during episodes of crustal thickening. In addition, another common feature among the Cordilleran batholiths is that they comprise mixed and homogenized melts that were extracted out of reservoirs located deeper than ~35 km. It appears that the main driver of silica enrichment in these batholiths, compared with more primitive island arcs, is garnet and to a lesser extent amphibole in the residual crustal assemblage.

Similar geochemical datasets exist for the modern Andes (Haschke *et al.*, 2002; Kay *et al.*, 2005, 2010; Mamani *et al.*, 2008, 2010). When comparing the two different exposure levels of these continental margin arcs, it is clear that coastal batholiths, like the CMB, represent near-perfect matches for the volcanic arcs of South America. The major and trace element characteristics discussed in this study are typical of the Andean volcanic chain, with the exception of the southernmost exposures where the upper plate is not compressional. For example, the Sr/Y ratios of most Andean arc magmatic rocks are high, corresponding to the field of 'adakites' (*sensu lato*) for intermediate compositions ($55\% < SiO_2 < 70\%$); this is a first-order parameter suggesting that magma generation took place at crustal levels deeper then the plagioclase stability field.

When comparing the CMB with other Cordilleran arc, it becomes obvious that similar magmatic fluxes and major element compositions are found in all arcs regardless of how 'primitive' the source materials are on average, as defined by the radiogenic isotope compositions. The process of generating large batholiths, multi-pluton aggregates that can comprise several million cubic kilometers in volume over 100 Myr timescales, is not dependent on the lithospheric age of the upper plate, despite the fact that the mass of the batholiths may comprise equal contributions from the mantle and crust. Interpretations regarding Cordilleran or Andean arc evolution at timescales of tens to hundreds of million years will have to acknowledge the cyclic evolution of magmatism in these arcs and their relationships to pulses of lithospheric thickening and thinning (and/or delamination) as proposed by the orogenic cycle model (DeCelles *et al.*, 2009) and its precursor ideas (e.g. Kay & Mpodozis, 2001).

CONCLUSIONS

(1) Major and trace element data indicate that 82 samples of the Coast Mountains Batholith, along three orogen-normal transects, are intermediate to felsic, calc-alkaline arc magmatic rocks. The average composition of the batholith integrated over the course of its >150 Myr life is more silicic than generally envisaged for 'arcs' in general (Christensen & Mooney, 1995; Rudnick & Fountain, 1995; Ducea *et al.*, 2003), straddling the boundary between andesite and dacite, despite the overall primitive isotopic compositions of the arc, when compared with the average of other large Cordilleran batholiths (Ducea & Barton, 2007).

(2) Eu anomalies allow some of the magmas to have equilibrated with residual plagioclase, or to have undergone plagioclase fractionation shallower than 35–40 km. However, most CMB magmas did not equilibrate with significant plagioclase, either as melting residues or as crystal fractionates. The main magmatic products seen at the surface today were extracted from depths in excess of 35–40 km below the surface at the time of arc formation and did not undergo much subsequent fractionation or assimilation. This domain of lower crustal depths in an area that most probably was characterized by crustal thicknesses in excess of 60 km during arc formation is equivalent to the MASH zone proposed for the subsurface underlying modern arc stratovolcanoes (Hildreth & Moorbath, 1988).

(3) Steepness of REE patterns from La to Yb and Lu suggests that garnet was an important residual phase during magma genesis. $(La/Yb)_N$ is ≤ 10 during periods of low magmatic flux, but higher (up to 45) during high-flux magmatism. We infer that during significant periods of high-flux magmatism at 120–80 and 60–50 Ma, deep crustal partial melting often left garnet-rich eclogite-facies residues, including amphibole eclogite and garnet pyroxenite.

(4) SiO_2 is negatively correlated with Sc, Y and the heavier REE Gd to Lu, suggesting that residual garnet is a main driver of magma composition, and was probably the main agent responsible for SiO_2 enrichment up to 65% and above. Amphibole is suspected to be an additional driver to higher silica, but is not the only low-silica mineral in the residue.

(5) Nd and Sr isotopes show variations that are correlated with REE abundances and magmatic flux. Low flux periods at 140–120 and 80–60 Ma are characterized by low $^{87}Sr/^{86}Sr$ (<0·704) and high ε_{Nd} (> +4) values. These values change to ranges of 0·7045–0·709 and +3 to −2 respectively during high-flux periods at 120–80 and 60–50 Ma. The isotopic data indicate that more varied, and generally older or evolved, crustal materials are part of the magma source assemblage during high-flux magmatic periods. The limited isotopic heterogeneity of the CMB precludes interpretations of the origin of these more evolved materials, whether they are derived by tectonic underplating from the trench side (Wetmore & Ducea, 2011) or from the foreland side (DeCelles *et al.*, 2009).

(6) Both REE abundances and Nd–Sr isotopes are distinct for the two segments of the Jurassic to earliest Cretaceous arc. The western segment, sited in Alexander terrane, shares geochemical features with later high-flux periods, but petrogenetic interpretations are complicated by the presence of ancient supracrustal rocks at the present erosion level. The eastern segment, sited in the Stikine terrane, has more juvenile isotopic signatures, and REE abundances suggesting a possible derivation from shallower crustal levels than much of the younger CMB.

ACKNOWLEDGEMENTS

We thank J. Fan for analyses of trace elements, and R. Kerrich, supervisor of the University of Saskatchewan ICP MS facility, which is funded by grants to Kerrich and a George McLeod endowment to the Department

of Geological Sciences. We thank J. Thole and K. Wirth, Macalester College for major element abundances. T. Kayzar contributed to field and laboratory efforts in early stages of this project. We thank Don Willson of Silverking Charters. The original paper was considerably improved by constructive reviews by Bob Kay, Oliver Nebel and Cal Barnes, and additional review and editorial handling by Ron Frost.

FUNDING

This work was funded by NSF Continental Dynamics grant EAR-0309885 to the University of Arizona (Ducea, Patchett and Gehrels), and EAR-0310011 (Rusmore).

SUPPLEMENTARY DATA

Supplementary Data for this paper are available at *Journal of Petrology* online.

REFERENCES

Anczkiewicz, R., Platt, J. P., Thirlwall, M. F. & Wakabayashi, J. (2004). Franciscan subduction off to a slow start: evidence from high-precision Lu–Hf garnet ages on high grade blocks. *Earth and Planetary Science Letters* **225**, 147–161.

Andronicos, C. L., Hollister, L. S., Davidson, C. & Chardon, D. (1999). Kinematics and tectonic significance of transpressive structures within the Coast plutonic complex, British Columbia. *Journal of Structural Geology* **21**, 229–243.

Andronicos, C. L., Chardon, D. H., Hollister, L. S., Gehrels, G. E. & Woodsworth, G. J. (2003). Strain partitioning in an obliquely convergent orogen, plutonism, and synorogenic collapse; Coast Mountains Batholith, British Columbia, Canada. *Tectonics* **22**, doi:10.1029/2001TC001312.

Armstrong, R. L. (1988). Mesozoic and early Cenozoic magmatic evolution of the Canadian Cordillera. In: Clark, S. P., Burchfiel, B. C. & Suppe, J. (eds) *Processes in Continental Lithospheric Deformation: Geological Society of America Special Paper 218*. Boulder, Colorado: Geological Society of America, pp. 55–91.

Barker, F. & Arth, J. G. (1984). Preliminary results, Central Gneiss Complex of the Coast Range Batholith, southeastern Alaska; the roots of a high-K, calc-alkaline arc? *Physics of the Earth and Planetary Interiors* **35**, 191–198.

Barnes, C. G., Snoke, A. W., Harper, G. D., Frost, C. D., McFadden, R. R., Bushey, J. C. & Barnes, M. A. W. (2006). Arc plutonism following regional thrusting; petrology and geochemistry of syn- and post-Nevadan plutons in the Siskiyou Mountains, Klamath Mountains province, California. In: Snoke, A. W. & Barnes, C. G. (eds) *Geological Studies in the Klamath Mountains Province, California and Oregon: A Volume in Honor of William P. Irwin: Geological Society of America Special Paper 410*. Boulder, Colorado: Geological Society of America, pp. 357–376.

Barton, M. D., Battles, D. A., Debout, G. E., Capo, R. C., Christensen, J. N., Davis, S. R., Hanson, R. B., Michelsen, C. J. & Trim, H. E. (1988). Mesozoic contact metamorphism in the Western United States. In: Ernst, W. G. (ed.) *Metamorphism and Crustal Evolution, Western Conterminous United States: Rubey Volume VII*. Englewood Cliffs, New Jersey: Prentice-Hall, pp. 110–178.

Behn, M. D. & Kelemen, P. B. (2006). Stability of arc lower crust: Insights from the Talkeetna arc section, south central Alaska, and the seismic structure of modern arcs. *Journal of Geophysical Research* **111**, B11207, doi:10.1029/12006JB004327.

Blundy, J. & Wood, B. (1994). Prediction of crystal–melt partition coefficients from elastic moduli. *Nature* **372**, 452–454.

Boghossian, N. D. & Gehrels, G. E. (2000). Nd isotopic signature of metasedimentary pendants in the Coast Mountains between Prince Rupert and Bella Coola, British Columbia. *Geological Society of America, Special Papers* **343**, 77–87.

Bouvier, A., Vervoort, J. D. & Patchett, P. J. (2008). The Lu–Hf and Sm–Nd isotopic composition of CHUR: Constraints from unequilibrated chondrites and implications for the bulk composition of terrestrial planets. *Earth and Planetary Science Letters* **273**, 48–57.

Brophy, J. G. (2008). A study of rare earth element (REE)–SiO_2 variations in felsic liquids generated by basalt fractionation and amphibolite melting; a potential test for discriminating between the two different processes. *Contributions to Mineralogy and Petrology* **156**, 337–357.

Brown, M. (2001). Crustal melting and granite magmatism; key issues. *Physics and Chemistry of the Earth, Part A: Solid Earth and Geodesy* **26**, 201–212.

Butler, R. F., Gehrels, G. E., Baldwin, S. L. & Davidson, C. (2002). Paleomagnetism and geochronology of the Ecstall Pluton in the Coast Mountains of British Columbia: Evidence for local deformation rather than large-scale transport. *Journal of Geophysical Research* **107**, doi:10.1029/2001JB000270.

Calkins, J. A., Zandt, G., Girardi, J., Dueker, K., Gehrels, G. E. & Ducea, M. N. (2010). Characterization of the crust of the Coast Mountains Batholith, British Columbia, from P to S converted seismic waves and petrologic modeling. *Earth and Planetary Science Letters* **289**, 145–155.

Castillo, P. R., Janney, P. E. & Solidum, R. U. (1999). Petrology and geochemistry of Camiguin Island, southern Philippines: Insights to the source of adakites and other lavas in a complex arc setting. *Contributions to Mineralogy and Petrology* **134**, 33–51.

Castro, A., Gerya, T., Garcia-Casco, A., Fernandez, C., Diaz-Alvarado, J., Moreno-Ventas, I. & Low, I. (2010). Melting relations of MORB–sediment mélanges in underplated mantle-wedge plumes; Implications for the origin of Cordilleran-type batholiths. *Journal of Petrology* **51**, 1267–1295.

Cecil, M. R., Gehrels, G., Patchett, J. & Ducea, M. (2011). U–Pb–Hf characterization of the central Coast Mountains batholith: Implications for petrogenesis and crustal architecture. *Lithosphere* **3**, 247–260.

Christensen, N. I. & Mooney, W. D. (1995). Seismic velocity structure and composition of the continental crust; a global view. *Journal of Geophysical Research* **100**, 9761–9788.

Conrad, W. K. & Kay, R.W. (1984). Ultramafic and mafic inclusions from Adak Island: crystallization history, and implications for the nature of primary magmas and crustal evolution in the Aleutian Arc. *Journal of Petrology* **25**, 88–125.

Crawford, M. L., Hollister, L. S. & Woodsworth, G. J. (1987). Crustal deformation and regional metamorphism across a terrane boundary, Coast Plutonic Complex, British Columbia. *Tectonics* **6**, 343–361.

Crawford, M. L., Klepeis, K. A., Gehrels, G. & Isachsen, C. (1999). Batholith emplacement at mid-crustal levels and its exhumation within an obliquely convergent margin. *Tectonophysics* **312**, 57–78.

Cui, Y. & Russell, J. K. (1995). Nd–Sr–Pb isotopic studies of the southern Coast Plutonic Complex, southwestern British Columbia. *Geological Society of America Bulletin* **107**, 127–138.

Davies, J. H. & Stevenson, D. J. (1992). Physical model of source region of subduction zone volcanics. *Journal of Geophysical Research* **97**, 2037–2070.

DeCelles, P. G., Ducea, M. N., Kapp, P. & Zandt, G. (2009). Cyclicity in Cordilleran orogenic systems. *Nature Geoscience* **2**, 251–257, doi:10.1038/ngeo1469.

Defant, M. J. & Drummond, M. S. (1990). Derivation of some modern arc magmas by melting of young subducted lithosphere. *Nature* **347**, 662–665.

DePaolo, D. J. (1981). Trace element and isotopic effects of combined wallrock assimilation and fractional crystallization. *Earth and Planetary Science Letters* **53**, 189–202.

Drake, M. J. & Weill, D. F. (1975). Partition of Sr, Ba, Ca, Y, Eu^{2+}, Eu^{3+}, and other REE between plagioclase feldspar and magmatic liquid; an experimental study. *Geochimica et Cosmochimica Acta* **39**, 689–712.

Drummond, M. S. & Defant, M. J. (1990). A model for trondhjemite–tonalite–dacite genesis and crustal growth via slab melting; Archean to modern comparisons. *Journal of Geophysical Research* **95**, 21503–21521.

Ducea, M. N. (2001). The California Arc; thick granitic batholiths, eclogitic residues, lithospheric-scale thrusting, and magmatic flare-ups. *GSA Today* **11**, 4–10.

Ducea, M. N. (2002). Constraints on the bulk composition and root foundering rates of continental arcs; a California arc perspective. *Journal of Geophysical Research* **107**, doi:10.1029/2001JB000643.

Ducea, M. N. & Barton, M. D. (2007). Igniting flare-up events in Cordilleran arcs. *Geology* **35**, 1047–1050.

Ducea, M. N. & Saleeby, J. B. (1996). Buoyancy sources for a large, unrooted mountain range, the Sierra Nevada, California; evidence from xenolith thermobarometry. *Journal of Geophysical Research* **101**, 8229–8244.

Ducea, M. N., Kidder, S. & Zandt, G. (2003). Arc composition at mid-crustal depths; insights from the Coast Ridge Belt, Santa Lucia Mountains, California. *Geophysical Research Letters* **30**, doi:10.1029/2002GL016297.

Ducea, M. N., Kidder, S., Chesley, J. T. & Saleeby, J. B. (2009). Tectonic underplating of trench sediments beneath magmatic arcs; the Central California example. *International Geology Review* **51**, 1–26.

Engebretson, D. C., Cox, A. & Gordon, R. G. (1985). *Relative Motions between Oceanic and Continental Plates in the Pacific Basin. Geological Society of America, Special Papers* **206**, 59.

Friedman, R. M., Mahoney, J. B. & Cui, Y. (1995). Magmatic evolution of the southern Coast Belt; constraints from Nd–Sr isotopic systematics and geochronology of the southern Coast plutonic complex. *Canadian Journal of Earth Sciences* **32**, 1681–1698.

Frost, B. R. & Frost, C. D. (1987). CO_2 melts and granulite metamorphism. *Nature* **327**, 503–506.

Frost, C. D. & O'Nions, R. K. (1985). Caledonian magma genesis and crustal recycling. *Journal of Petrology* **26**, 515–544.

Frost, B. R., Barnes, C. G., Collins, W. J., Arculus, R. J., Ellis, D. J. & Frost, C. D. (2001). A geochemical classification for granitic rocks. *Journal of Petrology* **42**, 2033–2048.

Fujimaki, H., Tatsumoto, M. & Aoki, K.-i. (1984). Partition coefficients of Hf, Zr, and REE between phenocrysts and groundmasses. *Journal of Geophysical Research* **89**, 662–672.

Gao, Y., Hou, Z., Kamber, B., Wei, R., Meng, X. & Zhao, R. (2007). Adakite-like porphyries from the southern Tibetan continental collision zones: evidence for slab melt metasomatism. *Contributions to Mineralogy and Petrology* **153**, 105–120.

Gehrels, G. E. & Boghossian, N. D. (2000). Reconnaissance geology and U–Pb geochronology of the west flank of the Coast Mountains between Bella Coola and Prince Rupert, coastal British Columbia. In: Stowell, H. H. & McClelland, W. C. (eds) *Tectonics of the Coast Mountains, SE Alaska and Coastal British Columbia: Geological Society of America Special Paper 343.* Boulder, Colorado: Geological Society of America, pp. 61–76.

Gehrels, G. E., McClelland, W. C., Samson, S. D., Patchett, P. J. & Jackson, J. L. (1990). Ancient continental margin assemblage in the northern Coast Mountains, southeast Alaska and northwest Canada. *Geology* **18**, 208–211.

Gehrels, G., Rusmore, M., Woodsworth, G., Crawford, M., Andronicos, C., Hollister, L., Patchett, J., Ducea, M., Butler, R., Klepeis, K., Davidson, C., Friedman, R., Haggart, J., Mahoney, B., Crawford, W., Pearson, D. & Girardi, J. (2009). U–Th–Pb geochronology of the Coast Mountains batholith in north-coastal British Columbia: Constraints on age and tectonic evolution. *Geological Society of America Bulletin* **121**, 1341–1361.

Gromet, L. P. & Silver, L. T. (1987). REE variations across the Peninsular Ranges Batholith; implications for batholithic petrogenesis and crustal growth in magmatic arcs. *Journal of Petrology* **28**, 75–125.

Grove, T. L., Elkins-Tanton, L. T., Parman, S. W., Chatterjee, N., Muentener, O. & Gaetani, G. A. (2003). Fractional crystallization and mantle-melting controls on calc-alkaline differentiation trends. *Contributions to Mineralogy and Petrology* **145**, 515–533.

Hacker, B. R., Peacock, S. M., Abers, G. A. & Holloway, S. (2003). Subduction factory 2. Intermediate-depth earthquakes in subducting slabs are linked to metamorphic dehydration reactions. *Journal of Geophysical Research* **108**, doi:10.1029/2001JB001129.

Hacker, B. R., Kelemen, P. B. & Behn, M. D. (2011). Differentiation of the continental crust by relamination. *Earth and Planetary Science Letters* **307**, 501–516.

Haeussler, P. J., Bradley, D. C., Wells, R. E. & Miller, M. L. (2003). Life and death of the Resurrection plate: Evidence for its existence and subduction in the northeastern Pacific in Paleocene–Eocene time. *Geological Society of America Bulletin* **115**, 867–880.

Haschke, M. R., Scheuber, E., Guenther, A. & Reutter, K. J. (2002). Evolutionary cycles during the Andean Orogeny; repeated slab breakoff and flat subduction? *Terra Nova* **14**, 49–55.

Heah, T. S. T. (1990). Eastern margin of the Central Gneiss Complex in the Shames River area, Terrace, British Columbia. *Current Research, Part E: Geological Survey of Canada* **90-1E**, 159–169.

Heah, T. S. T. (1991). Mesozoic, ductile shear and Paleogene extension along the eastern margin of the Central Gneiss Complex, Coast Belt, Shames River area, near Terrace, British Columbia, MS thesis, University of British Columbia, Vancouver, 155 p.

Hildreth, W. & Moorbath, S. (1988). Crustal contributions to arc magmatism in the Andes of central Chile. *Contributions to Mineralogy and Petrology* **98**, 455–489.

Hollister, L. S. (1982). Metamorphic evidence for rapid (2 mm/yr) uplift of a portion of the Central Gneiss Complex, Coast Mountains, B.C. *Canadian Mineralogist* **20**, 319–332.

Hollister, L. S. & Andronicos, C. L. (2000). The Central Gneiss Complex, Coast Mountains, British Columbia. In: Stowell, H. H. & McClelland, W. C. (eds) *Tectonics of the Coast Mountains, SE Alaska and British Columbia: Geological Society of America Special Paper 343.* Boulder, Colorado: Geological Society of America, pp. 45–59.

Hollister, L. S. & Andronicos, C. L. (2006). Formation of new continental crust in western British Columbia during transpression and transtension. *Earth and Planetary Science Letters* **249**, 29–38.

Hutchison, W. W. (1983). Geology of the Prince Rupert–Skeena map area, British Columbia. *Memoir of the Geological Survey of Canada* **294**, 116.

Irving, A. J. & Frey, F. A. (1978). Distribution of trace elements between garnet megacrysts and host volcanic liquids of kimberlitic to rhyolitic composition. *Geochimica et Cosmochimica Acta* **42**, 771–787.

Ito, K. & Kennedy, G. C. (1971). An experimental study of the basalt–garnet granulite–eclogite transition. In: Heacock, J. G. (ed.) *The Structure and Physical Properties of the Earth's Crust, Geophysical Monograph Series 14*. Washington, D. C.: American Geophysical Union, pp. 303–314.

Jagoutz, O., Müntener, O., Schmidt, M. W. & Burg, J. P. (2011). The roles of flux- and decompression melting and their respective fractionation lines for continental crust formation: Evidence from the Kohistan arc. *Earth and Planetary Science Letters* **303**, 25–36.

Jenner, G. A., Longerich, H. P., Jackson, S. E. & Fryer, B. J. (1990). ICP-MS; a powerful tool for high-precision trace-element analysis in earth sciences; evidence from analysis of selected U.S.G.S. reference samples. *Chemical Geology* **83**, 133–148.

Jull, M. & Kelemen, P. B. (2001). On the conditions for lower crustal convective instability. *Journal of Geophysical Research* **106**, 6423–6446.

Kapp, P. A. & Gehrels, G. E. (1998). Detrital zircon constraints on the tectonic evolution of the Gravina Belt, Southeastern Alaska. *Canadian Journal of Earth Sciences* **35**, 253–268.

Kay, R. W. (1978). Aleutian magnesian andesites; melts from subducted Pacific Ocean crust. *Journal of Volcanology and Geothermal Research* **4**, 117–132.

Kay, R. W. & Kay, S. M. (1988). Crustal recycling and the Aleutian arc. *Geochimica et Cosmochimica Acta* **52**, 1351–1359.

Kay, R. W. & Kay, S. M. (1991). Creation and destruction of the lower continental crust. *Geologische Rundschau* **80**, 250–270.

Kay, R. W. & Kay, S. M. (1993). Delamination and delamination magmatism. *Tectonophysics* **219**, 177–189.

Kay, S. M. & Mpodozis, C. (2001). Central Andean ore deposits linked to evolving shallow subduction systems and thickening crust. *GSA Today* **11**, 4–9.

Kay, S.M., Gody, E. & Kurz, A. (2005). Episodic arc migration, crustal thickening, subduction erosion and magmatism in the south–central Andes. *Geological Society of America Bulletin* **117**, 67–88.

Kay, S. M., Coira, B. L., Caffe, P. J. & Chen, C.-H. (2010). Regional chemical diversity, crustal and mantle sources and evolution of central Andean Puna Plateau ignimbrites. *Journal of Volcanology and Geothermal Research* **198**, 81–111.

Kelemen, P. B., Rilling, J. L., Parmentier, E. M., Mehl, L. & Hacker, B. R. (2003). Thermal structure due to solid-state flow in the mantle wedge beneath arcs. In: Eiler, J. (ed.) *Inside the Subduction Factory, Geophysical Monograph Series 138*. Washington, DC: American Geophysical Union, pp. 293–311.

Kistler, R. W. & Peterman, Z. E. (1973). Variations in Sr, Rb, K, Na, and initial Sr^{87}/Sr^{86} in Mesozoic granitic rocks and intruded wall rocks in central California. *Geological Society of America Bulletin* **84**, 3489–3512.

Kistler, R. W. & Peterman, Z. E. (1978). *Reconstruction of crustal blocks of California on the basis of initial strontium isotopic compositions of Mesozoic granitic rocks. US Geological Survey Professional Papers* **1071**, 17 pp.

Klein, M., Stosch, H. G. & Seck, H. A. (1997). Partitioning of high field-strength and rare-earth elements between amphibole and quartz-dioritic to tonalitic melts; an experimental study. *Chemical Geology* **138**, 257–271.

Klein, M., Stosch, H. G., Seck, H. A. & Shimizu, N. (2000). Experimental partitioning of high field strength and rare earth elements between clinopyroxene and garnet in andesitic to tonalitic systems. *Geochimica et Cosmochimica Acta* **64**, 99–115.

Lee, C.-T., Rudnick, R. L. & Brimhall, G. H. (2001). Deep lithospheric dynamics beneath the Sierra Nevada during the Mesozoic and Cenozoic as inferred from xenolith petrology. *Geochemistry, Geophysics, Geosystems* **2**, 1053, doi:10.1029/2001GC000152.

Longerich, H. P., Jenner, G. A., Fryer, B. J. & Jackson, S. E. (1990). Inductively coupled plasma-mass spectrometric analysis of geological samples; a critical evaluation based on case studies. *Chemical Geology* **83**, 105–118.

MacIntyre, D. G., Villeneuve, M. E. & Schiarizza, P. (2001). Timing and tectonic setting of Stikine Terrane magmatism, Babine–Takla lakes area, central British Columbia. *Canadian Journal of Earth Sciences* **38**, 579–601.

Mahoney, J. B., Gordee, S. M., Haggart, J. W., Friedman, R. M., Diakow, L. J. & Woodsworth, G. J. (2009). Magmatic evolution of the eastern Coast Plutonic Complex, Bella Coola region, west–central British Columbia. *Geological Society of America Bulletin* **121**, 1362–1380.

Mamani, M., Tassara, A. & Wörner, G. (2008). Composition and structural control of crustal domains in the central Andes. *Geochemistry, Geophysics, Geosystems* **9**, Q03006, doi:10.1029/02007GC001925.

Mamani, M., Worner, G. & Sempere, T. (2010). Geochemical variations in igneous rocks of the Central Andean orocline (13°S to 18°S): Tracing crustal thickening and magma generation through time and space. *Geological Society of America Bulletin* **122**, 162–182.

Manthei, C. D., Ducea, M. N., Girardi, J., Patchett, P. J. & Gehrels, G. E. (2010). Isotopic and geochemical evidence for a recent transition in mantle chemistry beneath the western Canadian Cordillera. *Journal of Geophysical Research* **115**, doi:10.1029/2009JB006562.

Mantle, G. W. & Collins, W. J. (2008). Quantifying crustal thickness variations in evolving orogens: Correlation between arc basalt composition and Moho depth. *Geology* **36**, 87–90.

Martin, H. (1993). The mechanisms of petrogenesis of the Archaean continental crust; comparison with modern processes. *Lithos* **30**, 373–388.

McClelland, W. C., Gehrels, G. E. & Saleeby, J. B. (1992). Upper Jurassic–Lower Cretaceous basinal strata along the Cordilleran margin; implications for the accretionary history of the Alexander–Wrangellia–Peninsular Terrane. *Tectonics* **11**, 823–835.

McCulloch, M. T. (1993). The role of subducted slabs in an evolving Earth. *Earth and Planetary Science Letters* **115**, 89–100.

McDonough, W. F. & Sun, S. S. (1995). The composition of the Earth. *Chemical Geology* **120**, 223–253.

McKay, G. A. (1989). Partitioning of rare earth elements between major silicate minerals and basaltic melts. In: Lipin, B. R. & McKay, G. A. (eds) *Geochemistry and Mineralogy of Rare Earth Elements, Reviews in Mineralogy 21*. Chantilly, Virginia: Mineralogical Society of America, pp. 45–77.

Monger, J. W. H. & Price, R. A. (2002). The Canadian Cordillera: geology and tectonic evolution. *CSEG Recorder* **27**, 17–36.

Monger, J. W. H., Price, R. A. & Tempelman-Kluit, D. J. (1982). Tectonic accretion and the origin of the two major metamorphic and plutonic welts in the Canadian Cordillera. *Geology* **10**, 70–75.

Monger, J. W. H., van der Heyden, P., Journeay, J. M., Evenchick, C. A. & Mahoney, J. B. (1994). Jurassic–Cretaceous basins along the Canadian Coast Belt: Their bearing on pre-mid-Cretaceous sinistral displacements. *Geology* **22**, 175–178.

Otamendi, J. E., Ducea, M. N., Tibaldi, A. M., Bergantz, G. W., de la Rosa, J. & Vujovich, G. I. (2009). Generation of tonalitic and dioritic magmas by coupled partial melting of gabbroic and metasedimentary rocks within the deep crust of the Famatinian magmatic arc, Argentina. *Journal of Petrology* **50**, 841–873.

Patchett, P. J. & Ruiz, J. (1987). Nd isotopic ages of crust formation and metamorphism in the Precambrian of eastern and southern Mexico. *Contributions to Mineralogy and Petrology* **96**, 523–528.

Patchett, P. J., Gehrels, G. E. & Isachsen, C. E. (1998). Nd isotopic characteristics of metamorphic and plutonic rocks of the Coast

Mountains near Prince Rupert, British Columbia. *Canadian Journal of Earth Sciences* **35**, 556–561.

Patiño-Douce, A. E., Humphreys, E. D. & Johnston, A. D. (1990). Anatexis and metamorphism in tectonically thickened continental crust exemplified by the Sevier hinterland, western North America. *Earth and Planetary Science Letters* **97**, 290–315.

Peacock, S. M. (1990). Fluid processes in subduction zones. *Science* **248**, 329–337.

Peacock, S. M. (1993). Large-scale hydration of the lithosphere above subducting slabs. *Chemical Geology* **108**, 49–59.

Pearce, J. A. (1983). Role of the sub-continental lithosphere in magma genesis at active continental margins. In: Hawkesworth, C. J. & Norry, M. J. (eds) *Continental Basalts and Mantle Xenoliths*. Nantwich: Shiva, pp. 230–249.

Pickett, D. A. & Saleeby, J. B. (1993). Thermobarometric constraints on the depth of exposure and conditions of plutonism and metamorphism at deep levels of the Sierra Nevada Batholith, Tehachapi Mountains, California. *Journal of Geophysical Research* **98**, 609–629.

Rapp, R. P. (1995). Amphibole-out phase boundary in partially melted metabasalt, its control over liquid fraction and composition, and source permeability. *Journal of Geophysical Research* **100**, 15601–15610.

Rapp, R. P. & Watson, E. B. (1995). Dehydration melting of metabasalt at 8–32 kbar; implications for continental growth and crust–mantle recycling. *Journal of Petrology* **36**, 891–931.

Reymer, A. & Schubert, G. (1984). Phanerozoic addition rates to the continental crust and crustal growth. *Tectonics* **3**, 63–77.

Richards, J. P. & Kerrich, R. (2007). Adakite-like rocks: their diverse origins and questionable role in metallogenesis. *Economic Geology* **102**, 537–576.

Rodriguez-Vargas, A., Koester, E., Mallmann, G., Conceição, R. V., Kawashita, K. & Weber, M. B. I. (2005). Mantle diversity beneath the Colombian Andes, Northern Volcanic Zone: Constraints from Sr and Nd isotopes. *Lithos* **82**, 471–484.

Romick, J. D., Kay, S. M. & Kay, R. W. (1992). The influence of amphibole fractionation on the evolution of calc-alkaline andesite and dacite tephra from the central Aleutians, Alaska. *Contributions to Mineralogy and Petrology* **112**, 101–118.

Rubin, C. M., Saleeby, J. B., Cowan, D. S., Brandon, M. T. & McGroder, M. F. (1990). Regionally extensive mid-Cretaceous west-vergent thrust system in the northwestern Cordillera: Implications for continent-margin tectonism. *Geology* **18**, 276–280.

Rudnick, R. L. & Fountain, D. M. (1995). Nature and composition of the continental crust; a lower crustal perspective. *Reviews of Geophysics* **33**, 267–309.

Rusmore, M. E. & Woodsworth, G. J. (1991). Coast Plutonic Complex: A mid-Cretaceous contractional orogen. *Geology* **19**, 941–944.

Rusmore, M. E. & Woodsworth, G. J. (1994). Evolution of the eastern Waddington thrust belt and its relation to the Mid-Cretaceous Coast Mountains arc, western British Columbia. *Tectonics* **13**, 1052–1067.

Rusmore, M. E., Gehrels, G. & Woodsworth, G. J. (2001). Southern continuation of the Coast shear zone and Paleocene strain partitioning in British Columbia–southeast Alaska. *Geological Society of America Bulletin* **113**, 961–975.

Rusmore, M. E., Woodsworth, G. J. & Gehrels, G. E. (2005). Two-stage exhumation of midcrustal arc rocks, Coast Mountains, British Columbia. *Tectonics* **24**, doi:10.1029/2004TC001750.

Rusmore, M. E., Gehrels, G. & Woodsworth, G. J. (2007). Crustal structure and magmatism, Coast Mountains Orogen, latitude 52–53 degrees north, British Columbia, Canada. *EOS, Transactions, American Geophysical Union* **88**(52), Fall Meeting Supplement, Abstract T11B-0582.

Saleeby, J. (2003). Segmentation of the Laramide Slab—evidence from the southern Sierra Nevada region. *Geological Society of America Bulletin* **115**, 655–668.

Saleeby, J. B., Ducea, M. N. & Clemens-Knott, D. (2003). Production and loss of high-density batholithic root, southern Sierra Nevada, California. *Tectonics* **22**, doi:10.1029/2002TC001374.

Samson, S. D. & Patchett, P. J. (1991). The Canadian Cordillera as a modern analogue of Proterozoic crustal growth. *Australian Journal of Earth Sciences* **38**, 595–611.

Samson, S. D., McClelland, W. C., Patchett, P. J., Gehrels, G. E. & Anderson, R. G. (1989). Evidence from neodymium isotopes for mantle contributions to Phanerozoic crustal genesis in the Canadian Cordillera. *Nature* **337**, 705–709.

Samson, S. D., Patchett, P. J., McClelland, W. C. & Gehrels, G. E. (1991*a*). Nd and Sr isotopic constraints on the petrogenesis of the west side of the northern Coast Mountains Batholith, Alaskan and Canadian Cordillera. *Canadian Journal of Earth Sciences* **28**, 939–946.

Samson, S. D., Patchett, P. J., McClelland, W. C. & Gehrels, G. E. (1991*b*). Nd isotopic characterization of metamorphic rocks in the Coast Mountains, Alaskan and Canadian Cordillera; ancient crust bounded by juvenile terranes. *Tectonics* **10**, 770–780.

Schmidt, M. W. & Poli, S. (1998). Experimentally based water budgets for dehydrating slabs and consequences for arc magma generation. *Earth and Planetary Science Letters* **163**, 361–379.

Schnetzler, C. C. & Philpotts, J. A. (1970). Partition coefficients of rare-earth elements between igneous matrix material and rock-forming mineral phenocrysts; II. *Geochimica et Cosmochimica Acta* **34**, 331–340.

Solar, G. S. & Brown, M. (2001). Petrogenesis of migmatites in Maine, USA; possible source of peraluminous leucogranite in plutons? *Journal of Petrology* **42**, 789–823.

Staudigel, H., Davies, G. R., Hart, S. R., Marchant, K. M. & Smith, B. M. (1995). Large scale isotopic Sr, Nd and O isotopic anatomy of altered oceanic crust; DSDP/ODP sites 417/418. *Earth and Planetary Science Letters* **130**, 169–185.

Stern, C.R. (2011). Subduction erosion: Rates, mechanisms, and its role in arc magmatism and the evolution of the continental crust and mantle. *Gondwana Research* **20**, 284–304.

Stern, C.R. & Kilian, R. (1996). Role of the subducted slab, mantle wedge and continental crust in the generation of adakites from the Andean Austral Volcanic Zone. *Contributions to Mineralogy and Petrology* **123**, 263–281.

Stolper, E. & Newman, S. (1994). The role of water in the petrogenesis of Mariana Trough magmas. *Earth and Planetary Science Letters* **121**, 293–325.

Taylor, H. P. (1980). The effects of assimilation of country rocks by magmas on $^{18}O/^{16}O$ and $^{87}Sr/^{86}Sr$ systematics in igneous rocks. *Earth and Planetary Science Letters* **47**, 243–254.

Thomas, J. B. & Sinha, A. K. (1999). Field, geochemical, and isotopic evidence for magma mixing and assimilation and fractional crystallization processes in the Quottoon igneous complex, northwestern British Columbia and Southeastern Alaska. *Canadian Journal of Earth Sciences* **36**, 819–831.

Tulloch, A. J. & Kimbrough, D. L. (2003). Paired plutonic belts in convergent margins and the development of high Sr/Y magmatism; Peninsular Ranges Batholith of Baja California and Median Batholith of New Zealand. In: Johnson, S. E., Paterson, S. R., Fletcher, J. M., Girty, G. H., Kimbrough, D. L. & Martin-Barajas, A. (eds) *Tectonic Evolution of Northwestern Mexico and the*

Southwestern USA: Geological Society of America Special Paper 374. Boulder, Colorado: Geological Society of America, pp. 275–295.

van der Heyden, P. (1992). A Middle Jurassic to early Tertiary Andean–Sierran arc model for the Coast Belt of British Columbia. *Tectonics* **11**, 82–97.

van Westrenen, W., Allan, N. L., Blundy, J. D., Purton, J. A. & Wood, B. J. (2000). Atomistic simulation of trace element incorporation into garnets; comparison with experimental garnet–melt partitioning data. *Geochimica et Cosmochimica Acta* **64**, 1629–1639.

Vervoort, J. D., Wirth, K., Kennedy, B., Sandland, T. & Harpp, K. S. (2007). The magmatic evolution of the Midcontinent Rift; new geochronologic and geochemical evidence from felsic magmatism. *Precambrian Research* **157**, 235–268.

Vielzeuf, D. & Holloway, J. R. (1988). Experimental determination of the fluid-absent melting relations in the pelitic system; consequences for crustal differentiation. *Contributions to Mineralogy and Petrology* **98**, 257–276.

Wetmore, P. H. & Ducea, M. N. (2011). Geochemical evidence of a near-surface history for source rocks of the central Coast Mountains Batholith, British Columbia. *International Geology Review* **51**, 1–26.

White, W. M. (1985). Sources of oceanic basalts: Radiogenic isotopic evidence. *Geology* **13**, 115–118.

Wolf, M. B. & Wyllie, P. J. (1993). Garnet growth during amphibolite anatexis; implications of a garnetiferous restite. *Journal of Geology* **101**, 357–373.

Wolf, M. B. & Wyllie, P. J. (1994). Dehydration-melting of amphibolite at 10 kbar; the effects of temperature and time. *Contributions to Mineralogy and Petrology* **115**, 369–383.

Wyllie, P. J. (1984). Constraints imposed by experimental petrology on possible and impossible magma sources and products. *Philosophical Transactions of the Royal Society of London, Series A* **310**, 439–456.

Zen, E.-a. & Hammarstrom, J. M. (1984). Magmatic epidote and its petrologic significance. *Geology* **12**, 515–518.